β_{hkl} is the peak width at half maximum intensity, in radians, of the hkl reflection in the WAXD patterns, and θ is the diffraction angle. Thus, the crystal characteristics of the iPP were little sensitive to the presence of elastomer or the molding conditions employed, in comparison with experimental error. The toughened iPP sample behaves as a compatible mixture with no evidence of mixing of the matrix and elastomer at the molecular level. Domain size was the principal variable determining impact toughness. A typical morphology of a compound with an iPP matrix is shown in figure 3.2.

Isotactic Poly(propylene-co-ethylene) Compounds

In the iPcE samples containing EOC1, the elastomer inclusions have several features that were not seen in the iPP samples; this is exemplified by the TEM micrograph of an iPcE compound in figure 3.3a. In figure 3.3b, an image with the contrast adjusted to emphasize the lamella texture in the matrix is shown. Lamellar crystals of comparable thickness to those seen in the continuous phase; i.e., in the range 10 to 11 nm, are located in the elastomer domains. While the elastomer is partially crystalline, possessing a nominal weight fraction crystallinity of less than 0.138 it has a broad melting endotherm covering the range 40 to 60°C, by DSC. This would not be consistent with a lamellar thickness of 10 nm. The weight fraction crystallinity, w_c, was determined:

$$\frac{1}{\rho} = \frac{w_c}{\rho_c} + \frac{(1 - w_c)}{\rho_a},$$

where ρ, ρ_c, and ρ_a are the total density, density of pure crystalline, orthorhombic, PE (1000 kgm^{-3} from X-ray analysis (12)), and the density of amorphous PE (854 kgm^{-3} from extrapolation of melt densities to 298 K(12)), respectively. Based upon the Gibbs-Thompson equation (13):

$$L_c = \frac{T_m^0 2\sigma_e}{(T_m^0 - T_m)\rho_c \Delta H^0},$$

considerably thinner crystals, with thickness, L_c, in the range, 2.5 to 3.1 nm, are anticipated; T^0_m is the equilibrium melting point of linear PE from the Hoffmann-Weekes method (415 K) (12), σ_e is fold surface energy of an orthorhombic PE crystal (90 mJm^{-2}) (12), T_m is the melting point, and ΔH^0 is the heat of fusion of an ideal orthorhombic PE crystal (293 Jg^{-1}) (12).

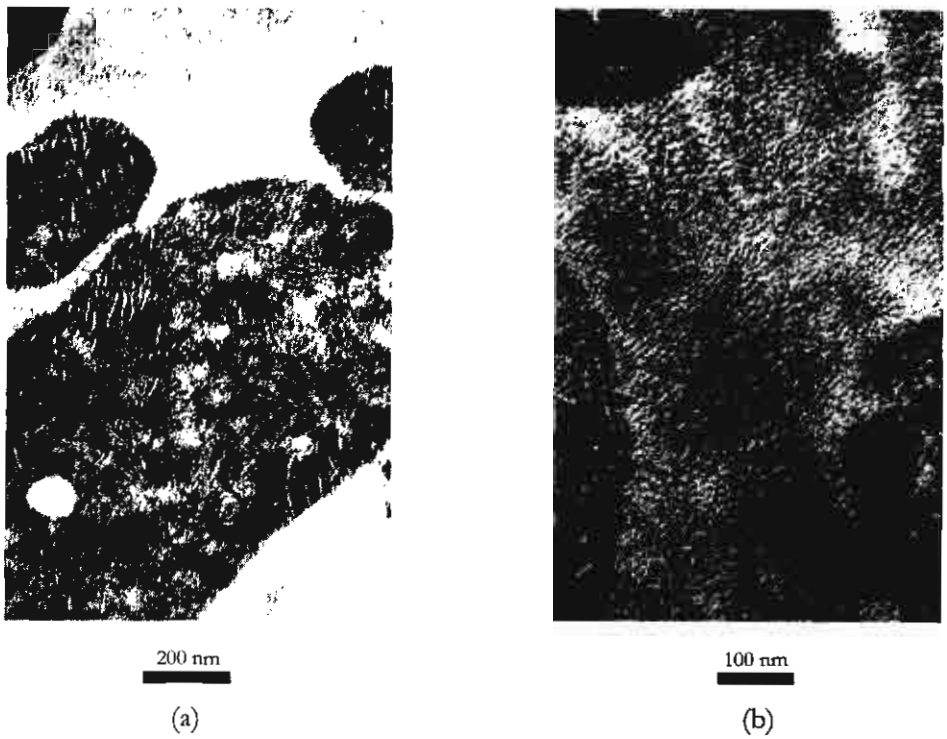

Figure 3.3 TEM micrographs of a PcE sample containing 30 wt% EOC1 injection molded at 170°C and 0 Pa back-pressure: (a) showing lamellar crystals in the elastomer domains; the white drop in the stained domain at bottom left is thought to be mechanically occluded matrix; (b) contrast adjusted to emphasize lamella texture of the matrix.

Moreover, the extensive chain branching and even branch distribution of the EOC may preclude the formation of regularly folded lamellar crystals since the elastomer possess, on average, one hexyl-branch per eight backbone carbon atoms. If σ_e = 62.5 mJm^{-2} (14), ρ_c = 936 kgm^{-3} (14), T^0_m = 461 K (14), and ΔH^0 = 207 Jg^{-1} (9) for an ideal monoclinic iPP crystal, the experimental melting point of 158°C (431 K) gives an anticipated lamellar thickness of 10 nm for the iPcE. It is therefore inferred that the lamellae in the elastomer domains comprise iPcE. The lamellae are less distinct in the matrix, because the iPcE-rich phase is less readily stained by the RuO_4 vapor although the characteristic crosshatched texture of iPP is discernable in figure 3.3b. The iPcE crystals are clearly seen within the elastomer domains in figure 3.3a, however, because they are lightly stained in contrast with the high concentration of highly stained EOC. It is reasonable to conclude that these lamellae were formed through the crystallization of iPcE that was dissolved in the EOC under the processing conditions. The dispersed domains in the iPcE samples containing 30 wt% (equivalent to 30.9 vol% at 298 K) of EOC injection molded at 170 and 230°C, with a back-pressure of 0 Pa, had mean domains sizes of 0.35 and 0.70 μm, respectively. Furthermore, the corresponding area fractions were 0.47 and 0.54, respectively. Thus, the area fractions are higher than would result from simple incorporation and dispersion of the elastomer into the matrix. The corresponding ligament lengths for these samples are thus 13 nm and zero.

The zero value is reached due to the assumption of simple cubic packing where the maximum packing fraction is 0.52; the real system, however, with random packing and polydisperse particle sizes will have larger ligament lengths than predicted. The Charpy impact energies at 0°C of these iPcE compounds were 10.0 kJm^{-2} and 4.7 kJm^{-2} for the samples injected molded at 170 and 230°C, respectively. The short ligament lengths resulting from an increase in the volume fraction of the elastomer-rich domains due to the incorporation of iPcE may reduce the effectiveness of the rubber toughening and also increase the probability, and hence rate, of dispersed droplet contact and coalescence. In this work, under no conditions could a single phase melt for this blend be prepared under quiescent conditions; that is, up to 350°C under nitrogen where embrittlement of the polymers became apparent. The morphology is thus thought to be a consequence of the partial mixing of the polymers under melt-flow.

A mottled texture of light and dark areas is seen in the elastomer domains of figure 3.3a due to an inhomogeneous RuO_4 staining in the section. This may result from the underlying distribution of elastomer and iPcE in the dispersed domains. The presence of the iPcE lamellae within the elastomer domains and the apparent immiscibility of the component polymers in the solid state, ascertained from the temperatures of the relaxation events through DMA, suggest partial mixing in the melt state followed by phase separation upon cooling. The mottled texture, indicating an inhomogeneous distribution of materials, may be the signature of liquid-liquid phase separation arrested, and frozen-in, by the crystallization of the iPcE. The spherical inclusion seen in the bottom left of figure 3.3a, of mean diameter 126 nm, is lightly stained material within the EOC domains. This feature is thought to be due to the presence of iPcE that was mechanically occluded during mixing, due to its regular shape and similar staining characteristics to the matrix phase, and hence the inclusions were probably not formed through phase separation.

Linear Polyethylene Samples

When the matrix was linear polyethylene, the morphology exemplified by the micrograph in figure 3.4 taken from a sample injection molded at 230°C containing 27.9 wt% of EOC2 (= 30 vol% at 25°C) was obtained. It comprises an interpenetrating morphology of elastomer domains and lamellar crystals of PE. The lamellae were measured from the TEM micrographs to be around 17 nm thick. A typical peak melting temperature, by DSC, of the blended PE, that was largely independent of elastomer contents lower than 30 wt%, was 129°C giving a predicted crystal thickness, according to the Gibbs-Thompson equation, of 19.6 nm; the data used in this calculation was the same as that used in the crystal thickness calculation of EOC. These results suggest that all lamellae situated in the EOC domains comprise linear PE, with no incorporation

of the elastomer into the crystals. The Jordhamo equation (15) for co-continuity of phases in immiscible systems is:

$$\frac{\eta_1}{\eta_2} \cdot \frac{\phi_2}{\phi_1} \cong 1,$$

where ϕ_i and η_i are the volume fraction and viscosity, respectively, of component i. The viscosity ratio, η_{EOC} / η_{PE}, of these polymers is of the order of 4 at most processing conditions used, and hence the co-continuity point of the phases would not be anticipated until the elastomer content approaches a maximum random packing fraction of the order of 0.72.

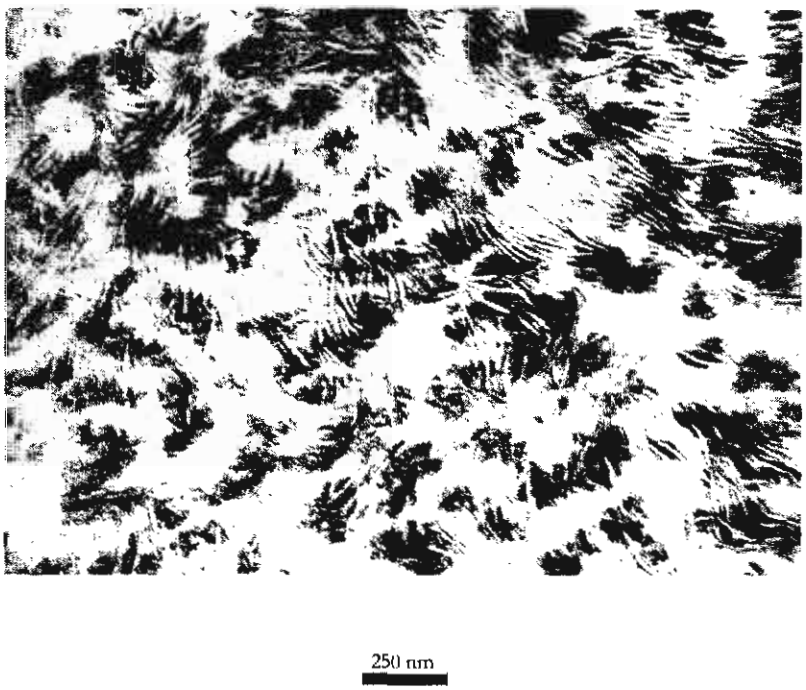

Figure 3.4 TEM micrograph showing the interpenetrating morphology found in the PE1 specimens, molded at 230°C and 0 Pa back pressure, containing 27.9 wt% of EOC2.

Evidently, however, much lower elastomer contents result in interconnected morphologies. From the extensive penetration of PE lamellar crystals into the EOC domains, it may be concluded that a considerable quantity of the PE and EOC were mixed at the molecular level at the onset of crystallization. The predicted critical composition, ϕ_2^c, from the Flory-Huggins lattice model (16),

$$\phi_2^c = \left(1 + \left(\nu_2 N_{w2} / \nu_1 N_{w1}\right)^{1/2}\right)^{-1},$$

is at 35.2 vol% of EOC2, at 25°C, in the case of PE2; where $N_{wi} = M_{wi}/M_{0i}$, M_{wi} is the weight average molecular weight, M_{0i} is the molecular weight of the polymer repeat unit, v_i is the molar volume of i at temperature, T, and subscript 1 and 2 refer to PE and EOC, respectively. Under the melt flow, conjugate PE-rich and elastomer-rich phases may be formed that are sheared to a very fine length of mixing that reaches the molecular level. The interpenetrating morphology must be a consequence of the phase separation after the flow of a partially miscible melt. DMA data showed that the major relaxation event of the EOC in the toughened PE moldings was only 5°C higher than the same process in the pure resins, implying that the component polymers were largely de-mixed at the molecular level in the solid state.

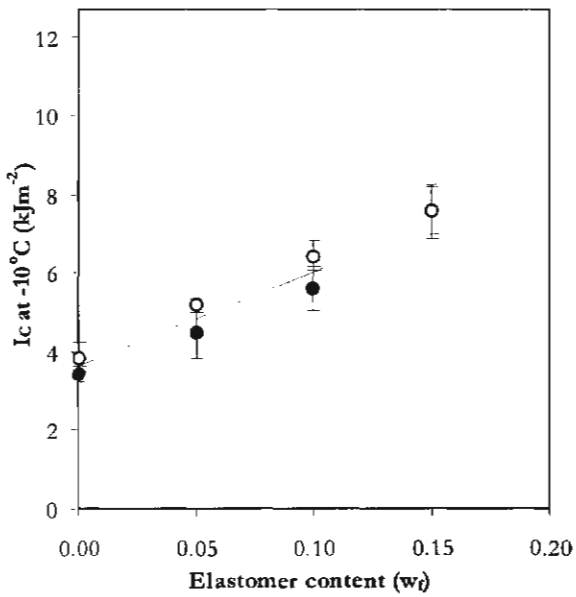

Figure 3.6 Charpy impact energies, I_C, at –10°C versus weight fraction of elastomer, w_f, for the EOC2 toughened PE2 samples injection molded at (●) 170 and (O) 230°C. Error bars are ± the sample standard deviation.

Under all molding conditions used, the melt must have been homogenized to a length-scale less than 170 nm. The coarsening processes during cooling generated the solid state morphology. Under quiescent conditions, the blend was found to be two-phase at the critical composition up to the limit of stability of the PE, that is around 375°C under a nitrogen atmosphere, and hence the critical temperature could not be determined. The injection molding conditions had a statistically significant, but technologically small, effect upon the impact properties of the PE samples, as shown in figure 3.5. In each condition, a very fine solid-state morphology of length-scale around 170 nm was obtained.

CONCLUSIONS

A range of solid-state morphologies were produced in the injection molded polyolefins toughened with poly(ethylene-co-1-octene) elastomer. The effect was thought to be related to the influence of melt-flow upon the partially miscible melt particularly when the ethylene content of the matrix was increased. Immiscibility in the solid state was found in each case, and hence it was inferred that the solid state morphologies were in part determined by the progress of phase separation and the concurrent crystallization of the matrix phase upon cooling after processing. For the iPP and iPcE systems, the impact properties were critically dependent upon the injection molding conditions, with decreases in toughness associated with increased elastomer domain sizes at higher molding temperatures. For the PE that exhibited pronounced miscibility in the melt-state, differences in the processing conditions had a relatively minor influence upon impact toughness.

REFERENCES

1. Walker, I.; Collyer, A. A. Rubber Toughening Mechanisms in Polymeric Materials. In *Rubber Toughened Engineering Plastics*, 1st Ed.; Collyer, A. A. Ed.; Chapman and Hall: London, 1994; 29-53.

2. Madbouly, S.; Ohmomo, M.; Ouzigawa, T.; Inoue, T. Polymer **1999**, *40*, 1465.

3. Kammer, H. W; Kummerlowe, C.; Kressler, J.; Melior, J. P. Polymer **1991**, *32* (8), 1488.

4. Inoue, T. Shear Induced Mixing in Polymer Blends. A Special Seminar Presented at the Faculty of Science, Mahidol University, Thailand, December 14th 1998.

5. Olley, R. H.; Basset, D. C. Polymer Communications **1982**, *23*, 1707.

6. Morton-Jones, D. H. Mixing. In *Polymer Processing*, 1st Ed.; Chapman and Hall: London, 1989; 71.

7. Rauwendaal C. Important Polymer Properties. In *Polymer Extrusion*, 2nd Ed.; Hanser Publishers: Munich, 1990; 181.

8. Wu, S. J. Appl. Polym. Sci. **1988**, *35*, 549.

9. Varga, J. Crystallization, Melting, and Supermolecular Structure of Isotactic Polypropylene. In *Polypropylene Structure, Blends, and Composites: Volume 1 Structure and Morphology*, 1st Ed.; Karger-Kocsis, J., Ed.; Chapman and Hall: London, 1995; Vol. 1, 64.

10. Cheng, S. Z. D.; Janimak, J. J.; Rodriguez, J. Crystalline Structures of Polypropylene Homo- and Copolymers. In *Polypropylene Structure, Blends, and Composites: Volume 1 Structure and Morphology*, 1st Ed.; Karger-Kocsis, J., Ed.; Chapman and Hall: London, 1995; Vol. 1, 38.

11. Snyder, R. L. X-Ray Diffraction. In *Materials Science and Technology: A Comprehensive Treatment: Volume 2A Characterisation of Materials Part I*, 1st Ed.; Lifshin, E., Ed.; VCH Verlagsgesellschaft: Weinheim, 1992; Vol. 2A, 290.

12. Gedde, U. W. *Polymer Physics*, Chapman and Hall: London, 1995.

13. Wunderlich, B., The Growth of Crystals. In *Macromolecular Physics: Volume 2: Crystal Nucleation, Growth, Annealing*, 1st Ed.; Academic Press: New York, 1976; Vol. 2, 154.

14. Varga, J. Crystallization, Melting, and Supermolecular Structure of Isotactic Polypropylene. In *Polypropylene Structure, Blends, and Composites: Volume 1 Structure and Morphology*, 1st Ed.; Karger-Kocsis, J., Ed.; Chapman and Hall: London, 1995; Vol. 1, 59.

15. Jordhamo, G. M.; Manson, J. A.; Sperling, L. H. Polym. Eng. Sci., **1986**, *26*, 517.

16. Crist, B.; Hill, M. J. Polymer, **1997**, *35*, 2329.

Results Part 4

Upon the morphology and toughness of a partially miscible high-density polyethylene / poly(ethylene-co-1-octene) blend

Abstract

Blends of linear polyethylene [PE] and an elastomeric poly(ethylene-co-1-octene) [EOC], containing 7 mol% octene, were found to be partially miscible in the melt-state and largely immiscible in the solid-state. Miscibility in the melt-state was inferred from the larger area fraction of EOC-rich domains in the solid-state than would be possible if the polymeric components remained in unmixed phases; moreover, PE lamella crystal were located within EOC domains. Processing history was found to have a marked effect upon the subsequent morphology formation, with higher processing temperatures leading to slower coarsening in subsequent operations. Maps of morphology, from micrographs of quenched annealed samples, versus composition and temperature suggested enhanced compatibility at elevated temperatures. Domains increased in size at a faster rate after melt-processing at 170°C than at 230°C leading to coarser morphologies for samples prepared at the lower temperature. Sample preparation under the former conditions led to superior impact toughness at –10°C than the latter.

INTRODUCTION

Polyolefin blends are finely balanced between miscibility and immiscibility [1]. The immiscibility may be related to the differences in chain conformation, which are affected by the type and quantities of chain branching [2] that lead to the reduction of the entropy change of mixing [3-7]. Relatively low levels of chain branching in one polymer may lead to immiscibility in the melt state under quiescent conditions [8]. The interaction between the state of miscibility in the melt and processing conditions controls the development of morphology in the solid-state, and consequently the properties of the material. A number of studies have reported the inferred partial miscibility in polypropylene based blends [9-11], but fewer studies have shown evidence for miscibility in polyethylene / elastomer blends [12]. In this report, the melt-state phase behaviour of a linear high-density polyethylene (PE) / highly branched elastomeric poly(ethylene-co-1-octene) (EOC) blend is described. A correlation between impact toughness, at –10°C, and the melt-state phase behaviour of moulded specimens is presented.

HDPE possessing a melt flow index of 14 g/10min and EOC with a melt flow index of 0.5 g/10min. The characteristics of these materials, and data used in the calculations in the discussion section, are documented in table 1.

The samples were prepared using a Prism 16 mm twin-screw extruder at a barrel temperature of 180°C and screw speed of 175 rpm. Volume fraction and weight fraction concentrations were inter-converted based upon the resin densities at 25°C, shown in table 1. Specimens of varying composition were annealed in an oil bath, after wrapping in aluminium foil, for 6 hrs at temperatures in the range 150 to 250°C. For higher temperatures, the specimens were heated in a tube furnace under nitrogen flow for 1 hr. A thermocouple was inserted in the sample to monitor the temperature.

Table 1. Resin characteristics and data

	Polyethylene	Poly(1-octene)	Poly(ethene-co-1-octene)
$V_{(25°C)}$ (cm^3mol^{-1})[a]	33.1	130.8	57.5[b]
$\rho_{(25°C)}$ (g/cm^3)[c]	0.962	-	0.868
T_m (°C)[d]	128	-	50
T_g (°C)	-20[e]	-91	-30[f]
M_w (g/mol)[g]	48,000	-	162,700
X	1,711	-	3,314
Octene content (mol%)	0	100	7[h]

[a]Amorphous phase only from ref. [13];
[b]Data calculated from the mole fraction weighted average of the values for polyethylene and poly(1-octene) from ref. [13];
[c]Includes amorphous and crystalline phases;
[d]DSC, this work;
[e]From the extrapolation to zero co-monomer content of a plot of T_g versus 1-butene content, using the data of ref. [9] and [16];
[f]DMA, this work;
[g]From data of manufacturer;
[h]^{13}C-NMR spectroscopy [14].

Ruthenium tetraoxide stained sections were viewed using an Hitachi H-300 transmission electron microscope. Flat surfaces, prepared with a cryo-ultramicrotome, were treated with a permanganic acid reagent [15] to selectively etch the amorphous material and then viewed using a scanning electron microscope (SEM) after coating with metal. Image analysis of the micrographs was carried out using Image Pro software upon digitised and calibrated images. Differential scanning calorimeter (DSC) data were obtained with a Perkin Elmer DSC7 instrument: specimens (10 mg ± 0.1 mg) were cut from the central core of the mouldings and dipped in silicone oil to ensure rapid heat transfer to the specimens. Fusion endotherms were obtained at a heating rate of 30°C/min, to limit annealing during heating, under a nitrogen atmosphere. Dynamic mechanical analyses were carried out using a Polymer Laboratories DMTA mkII instrument in tensile mode

at a deformation frequency of 10 Hz and heating rate of 5°C/min. Compression mouldings were prepared by firstly forming the specimens in an injection mould at 170 or 230°C followed by annealing for 5 min under atmospheric pressure on a compression platen at the same temperature. Finally, the mould was rapidly transferred to a water-cooled press at approximately 30°C and 150 psi. The specimens were tested using a Charpy pendulum impact tester, after conditioning in a water / ethylene glycol mixture at -10°C.

RESULTS AND DISCUSSION

Melt-state phase behaviour

The direct observation of morphology development in the melts of polyolefin blends is hampered by the small refractive index differences between the polymers. In this work, the samples appeared to be uniform at all conditions through direct observation of the melt. Upon rapid crystallisation of the PE, the melt phase morphology could be partially frozen-in, however. The length-scale of the features seen may be used to infer the state of the melt from the following reasoning. The self-diffusion distance, x, of a molecule diffusing in a melt of similar material may be estimated from $x^2 = 2D\Delta t$ and $D = 14 \times 10^{-6} M^{-2}$, where M is the molecular weight and t is time. From this analysis, the order of magnitude of the size of the phase dimensions expected during a 5 second quench from a homogeneous melt would be around 100 nm. Thus, an apparent state of the melt may be inferred. The true thermodynamic stability is not necessarily determined, however, only the homgeneity of the morphology is obtained.

Figure 4.1 shows micrographs of the samples that were annealed for six hours, quenched, microtomed, and then etched with permanganic acid. In figure 4.1(a), large circular holes up to 5 μm in diameter; i.e. an order of magnitude larger than that expected through quenching from a homogeneous melt, have been etched into the surface. The locations of the holes show the distribution of the EOC-rich phase. Moreover, the domains increased in size upon annealing for longer times, and hence from these observations it may be inferred that the blend was in a two-phase state, at the annealing condition.

Figure 4.1(b) shows a fine dispersed phase morphology, comprising holes with mean diameter of 0.33 μm left by etched domains of low crystallinity material; they are distributed in a continuous PE-rich phase that exhibits a banded spherulitic texture. The area fraction of the holes in the cross-section of the sample is 3.2%. If the area fraction is approximately equal to the volume fraction of the dispersed domains in the melt, the observed volume fraction is considerably lower than the 16.4 $vol\%_{(25°C)}$ total EOC content in the blend. In the melt-sate, the component polymers must have been partially mixed, forming a PE-rich majority α-phase and a minority EOC-rich β-phase. Using the 'lever rule', i.e.

$$\frac{\phi_\alpha}{\phi_\beta} = \frac{l}{l'} \quad \text{or} \quad \phi_\beta = \left(\frac{l}{l'+l}\right) \qquad [1]$$

where ϕ_i is the volume fraction of phase i and l is the length of tie-line in the phase diagram, it may be concluded that this condition must be close to the binodal locus.

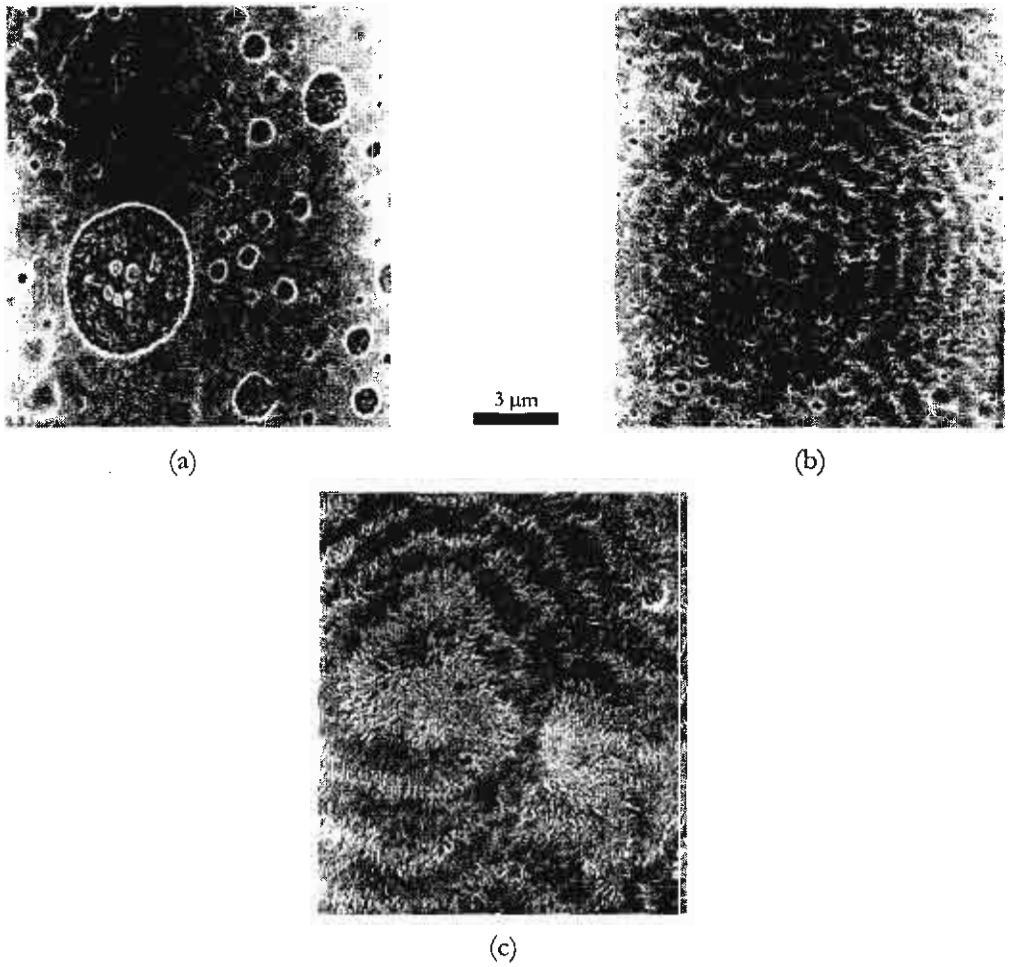

Figure 4.1 SEM micrographs of permanganic acid etched, microtomed surfaces. Samples were annealed in the melt for six hours at 230°C and then quenched: (a) 80:20 w/w; (b) 85:15 w/w, and (c) 90:10 w/w PE / EOC blend.

Moreover, the measured area fraction of the sample containing 21.7 vol% of elastomer annealed at 230°C was 11.8%. Near the cloud point, the volume fraction of the β-phase, ϕ_β, is low and the thermodynamic driving force to coarsen the morphology is weak, and hence the rate of coalescence of the droplets to form large domains is slow. Consequently, the observed domains are small. The morphology in figure 4.1(c) is essentially the same as that of the pure PE. No holes left by etched EOC-rich domains are discernible at this magnification. Inspection at higher magnifications revealed the presence of very small, etched domains, typically 150 nm in diameter,

intertwined with the PE crystalline fibrils. The width of the fibrils lie in the range 150 to 200 nm and consequently must consist of 10 to 12 lamellae that are around 17 nm (from TEM) across the fold surface. The dimensions of the etched domains are consistent with the suggestion that the EOC-rich domains were formed through phase separation from a melt that was homogeneous before quenching. Homogeneity may be concluded at least at the microscopic level, although not necessarily at the molecular level. The spherulitic morphology of the HDPE is little affected by the presence of the dissolved elastomer, since spherulites with diameters in the range 5 to 7 μm comprising up to five bands are obtained regardless of the presence of elastomer. For samples with EOC contents of 20 vol% and higher the spherulitic texture is obscured by the holes in the etched samples, phase contrast optical microscopy showed that the overall semi-crystalline texture was comparable with the samples containing lower EOC concentrations.

The intermixing of the two polymers in the melt-state may be further illustrated through consideration of the analysis of the TEM images in figure 4.2.

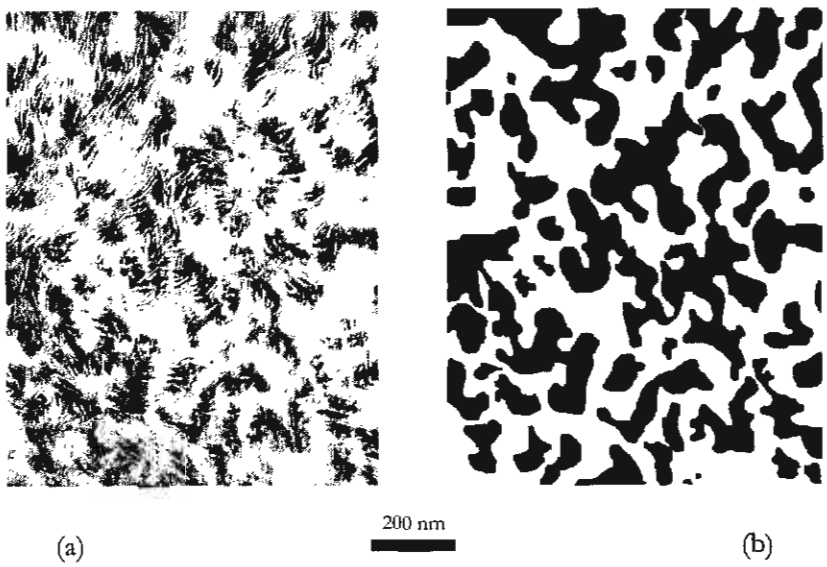

Figure 4.2 Images of a 70/30 w/w PE/EOC blend injection moulded at 230°C: (a) original TEM micrograph and (b) image after outlining of the EOC domains; area fraction is 0.47.

Figure 4.2(a) shows a TEM photomicrograph of a PE / EOC sample injection moulded at 230°C. Figure 4.2(b) is the same image, except that the EOC-rich regions have been filled in black and the PE-rich regions filled in white to produce a binary image of the TEM micrograph. The area fractions of the two regions were then determined using Image analysis. The area fraction of the EOC regions was found to be 47%, and hence the PE-rich areas constitute 53%. The content of EOC in the blend was 30%. Apparently, the location of the PE lamella crystals in the EOC-rich domains increases the effective area fraction of EOC. It is inferred from this observation that a fraction of the PE was dissolved in the EOC at the onset of crystallization.

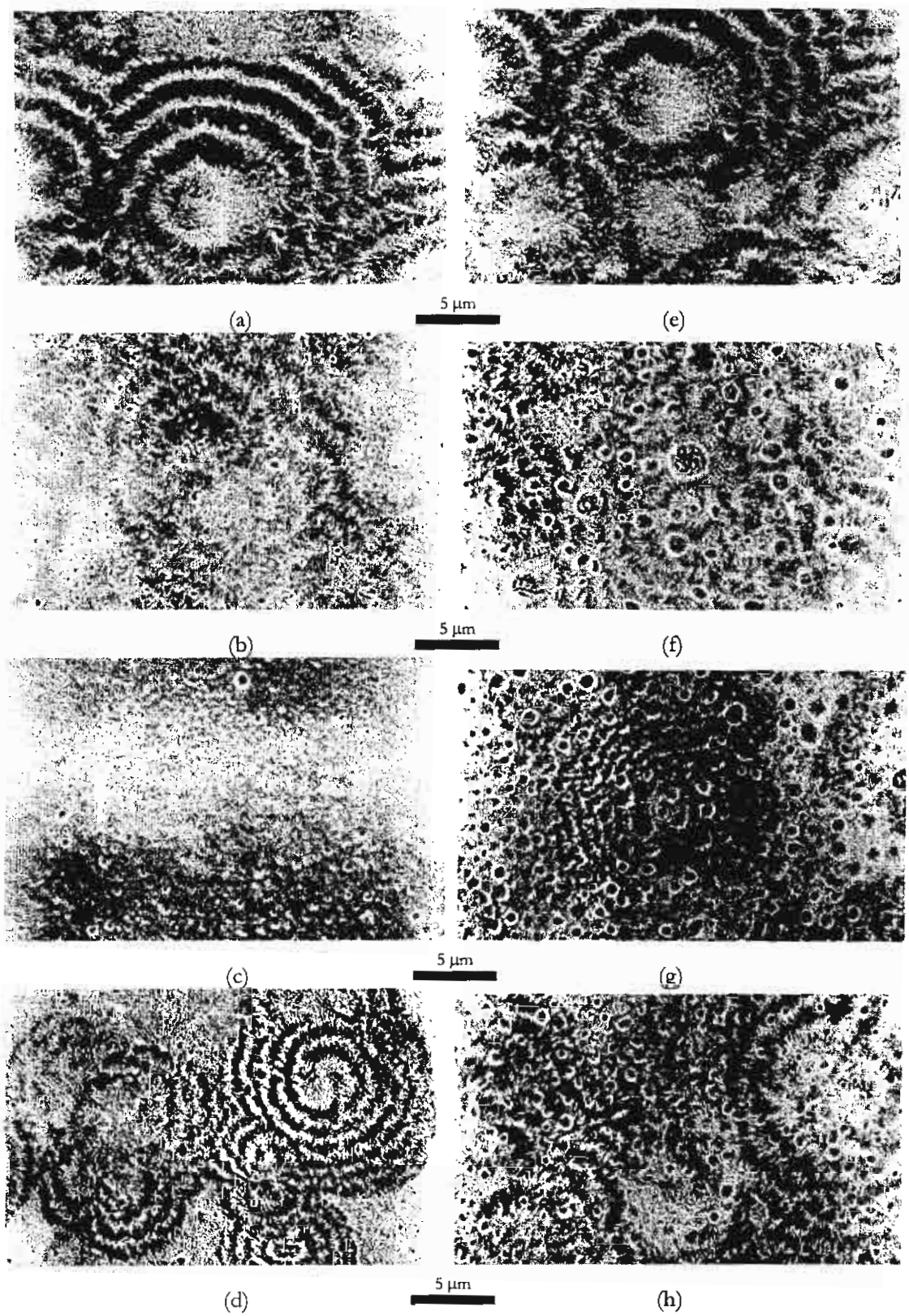

Figure 4.1 SEM micrographs of permanganic acid etched, microtomed surfaces of quenched specimens: (a) and (e) PE resin; PE / EO 80:20 w/w blend injection moulded at 230°C then annealed at (b) 285, (c) 300, and (d) 320°C, and moulded at 170°C then annealed at (f) 285, (g) 300, and (h) 320°C.

The morphology observations of the annealed samples prepared at 170 and 230°C and annealed at various temperatures are summarised in the diagram in figure 4.3, where the samples have been classified according to the observed length-scale of the etched domains.

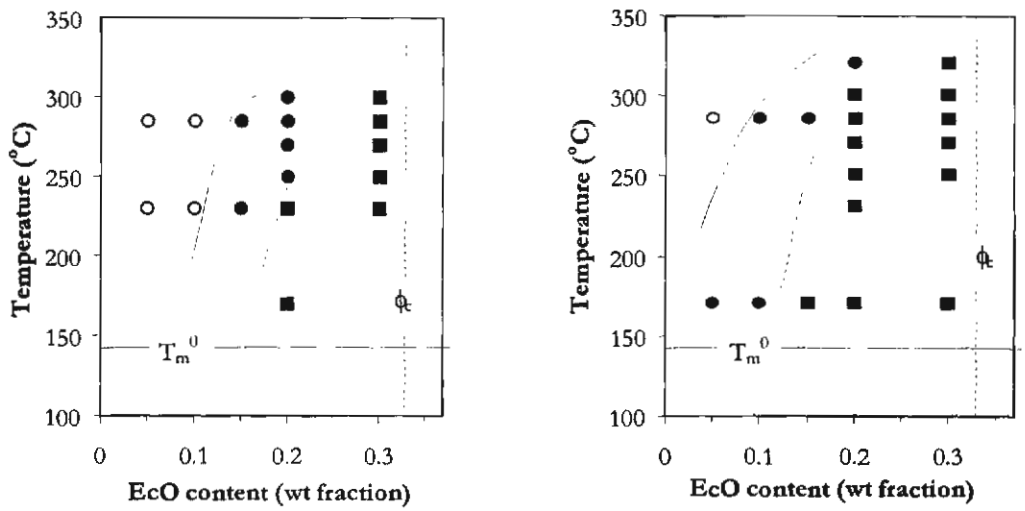

(a) (b)

Figure 4.3 'Morphology map' of the annealed samples based upon mean domain size, D_n: (●) 1 μm < D_n < 30 μm; (◆) 200 nm < D_n < 1 μm, and (O) D_n < 200 nm. T_m and T_c were determined through DSC analysis; boundary curves were drawn arbitrarily. Samples prepared at (a) 170 and (b) 230°C.

The critical composition, ϕ_c, was calculated from the Flory-Huggins lattice theory, employing the data in table 1:

$$\phi_{Min}^{c} = \left(1 + \left(\frac{v_{Min} x_{wMin}}{v_{Maj} x_{wMaj}}\right)^{1/2}\right)^{-1} \qquad [3]$$

where x_{wi} and v_i are the degree of polymerisation and molar volume, respectively, of species i. v_{EOC} was calculated from the mole fraction weighted average of the values for PE and poly(1-octene).

From figure 4.3 it can be seen that for both the samples prepared at 170 and 230°C the EOC-rich domains become smaller as the content of EOC decreases and as the temperature increases. The former observation is due to the reduction in the rate of coalescence as a consequence of fewer domain contacts as the quantity of EOC decreases. The reduced domain size at elevated temperatures shows that the greater thermal energy enhances the compatibility of

the blend components. Increased thermal energy reduces the melt viscosity. This alone would increase the domain size due to accelerated rates of coalescence, and therefore the enhancement in compatibility overrides the effect of reduced viscosity. Comparison of the morphology map of the samples prepared at 170 and 230°C shows that for every temperature and composition the samples processed at 230°C have a finer morphology than the equivalent formulation prepared at 170°C. This shows that even after annealing period of six hours, the processing history still has a pronounced effect upon the morphology that is subsequently formed. The enhanced compatibility that results from melt-processing at high temperature is maintained during subsequent thermal processing.

The length scales and area fractions of the domain morphologies reflect the partial miscibility of the blend that is enhanced at elevated temperature and suggest the underlying phase behaviour, although not necessarily the equilibrium condition. Extrapolation of the arbitrarily drawn boundary lines to the critical volume fraction suggest a critical point that is higher than 350°C, that is some way above the melt-processing window and into the region of rapid degradation of the polyethylene. Thus, the morphology diagram suggests upper critical solution temperature-type phase behaviour, although an hourglass shaped binodal locus extending to very high temperatures where the polymer degrades is also possible.

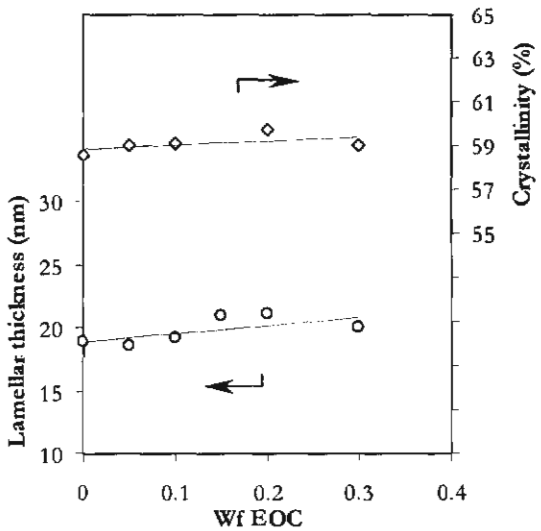

Figure 4.4 Crystallinity (◇) and lamella thickness (o) calculated from DSC data for the samples prepared at 230°C; data for the samples prepared at 170°C showed essentially the same result

Crystalline characteristics, determined from DSC analyses, are represented in figure 4.4; lamellar thickness, L_c, was calculated using the Thompson-Gibbs equation:

$$T_m = T_m^0\left(1 - \frac{2\sigma}{L_c \rho \Delta H^0}\right) \qquad [2]$$

where T_m is the melting point, T_m^0 is the equilibrium melting point, ΔH^0 is the heat of fusion, ρ is the crystal density, and σ is surface energy. The melt state phase behaviour does not greatly affect the PE crystallinity or lamellar thickness, under the conditions of sample preparation, within the experimental error of the DSC analyses, as shown in figure 4.4. Typical lamellar thickness, calculated from the Thompson-Gibbs equation, of around 20 nm was slightly higher than the 17 nm value obtained through TEM observations of stained sections.

Correlation of phase morphology with impact properties

Specimens were compression moulded in at 170 and 230°C. The corresponding impact energies, at –10°C, of these specimens are shown in figure 4.5; samples containing 20 wt% and higher EOC contents failed by hinging due to crack arrest. It is apparent that upon moving further into the immiscible region of the morphology diagram, either by reducing temperature or by increasing the EOC content, there are increases in the impact toughness of the blends.

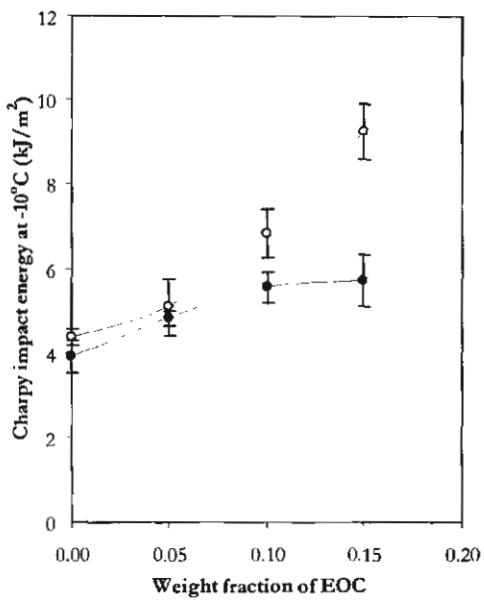

Figure 4.5 Relationship between the impact energy at –10°C and EOC content. Specimens compression moulded at (O) 170°C and (●) 230°C; error bars are the mean ± one standard deviation.

Representative morphologies of microtomed and permanganic acid etched specimens, moulded at condition 170 and 230°C, are shown in figure 4.6. Representative binarised images of these micrographs are shown in figure 4.7.

The mean EOC-rich domain size of the etched impact specimens is plotted as a function of EOC content in figure 4.8a; the impact energies are plotted against EOC-rich mean domain size in figure 4.8b. Both higher EOC contents and lower processing temperature lead to coarsening of the EOC-rich domains in the melt state. Higher quantities of elastomer lead to an increased frequency of droplet contact and coalescence, whereas lower temperatures confer a greater thermodynamic driving force, although lower kinetic mobility, to coarsen the morphology. When plotted against EOC-rich mean domain size, or average inter-particle distance, I_{dn}, from:

$$I_{dn} = D_n \Big/ \left[\left(\frac{\pi}{6\phi_{EO}} \right)^{1/3} - 1 \right]$$

the impact data do not fall on a single mastercurve, as is sometimes observed for rubber toughened matrices; a distinct curve is obtained for each moulding temperature. The impact toughness is affected not only by the domain size but also by the dispersed phase composition and volume fraction. All three factors are influenced by moulding temperature and total elastomer content.

Samples moulded near to the binodal condition have low volume fractions of the EOC-rich phase, although these may not be the equilibrium values due to the processing time of 5 minutes. Consequently, the larger fraction of the elastomer is dissolved in the PE-rich phase. Upon cooling, the system moves deeper into the spinodal region and the elastomer further separates from the PE in the melt state. Due to the extensive branching in the EOC, upon crystallisation of the PE it is excluded from the rapidly growing lamellae and collects in 150 nm domains in the inter-fibrillar regions of the PE spherulites. DMA showed that there was a slight increase in the T_g of EOC in the blends cooled rapidly from the melt, in comparison with the original EOC. This 5 to 7°C change was insensitive to melt temperature or blend composition, however. If the T_g of linear PE were taken as -20°C (16) [although this value is not universally accepted], this result would be consistent with the presence of an EOC-rich phase in the solid-state containing a small amount of amorphous polyethylene. Linear polyethylene does not show a clear transition at -20°C, and so the T_g of the conjugate PE-rich phase could not be determined. Thus, in the solid-state, the blend components largely exist in separate domains of amorphous PE, crystalline PE, and amorphous elastomer.

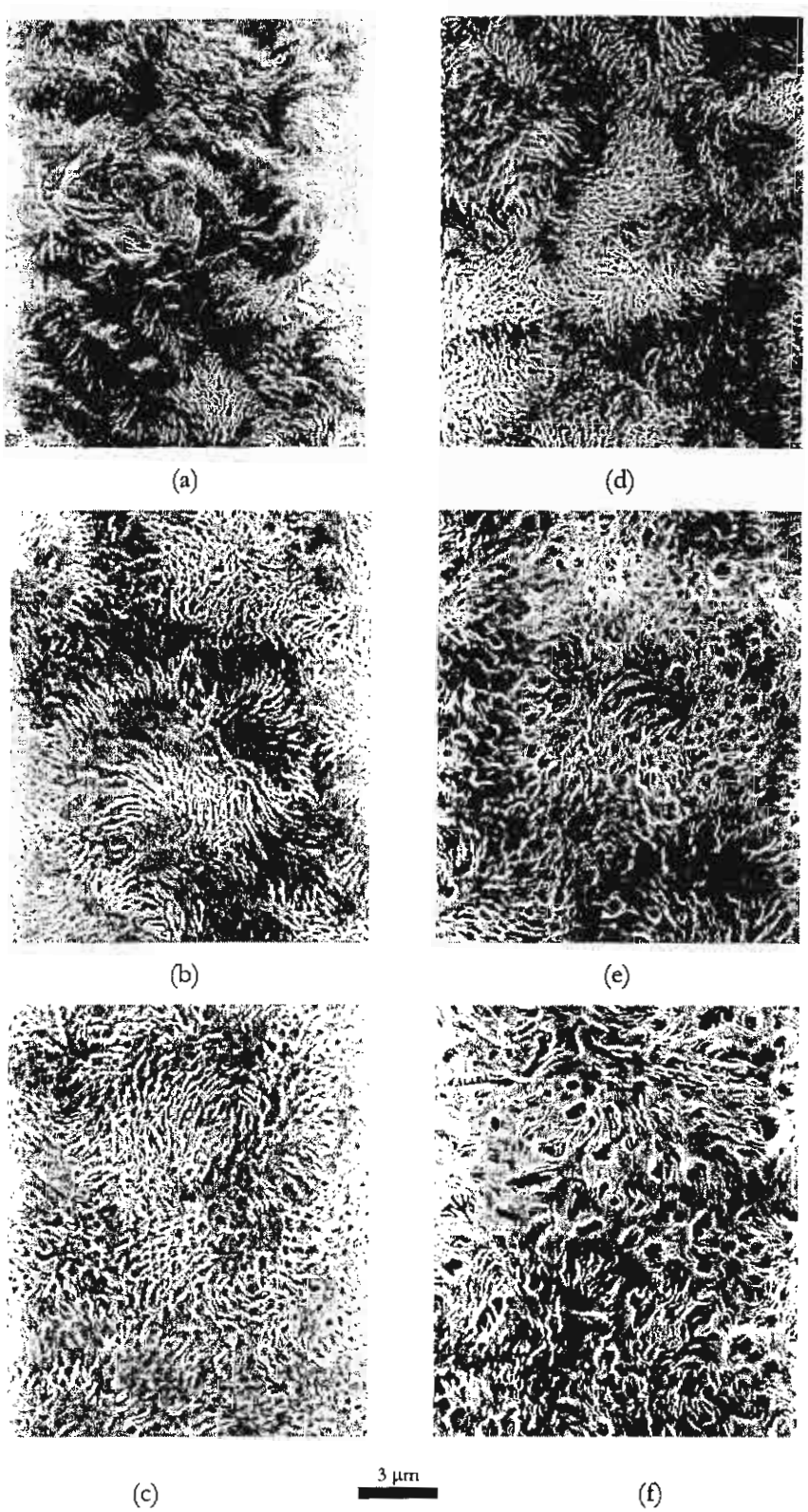

Figure 4.6 SEM micrographs showing the morphologies of the compression moulded impact specimens containing 10, 15, and 20 wt% EOC moulded at (a), (b), and (c) 230°C and (d), (e),

and (f) 170°C for 5 min. Surfaces were prepared through microtomy followed by permanganic acid etching.

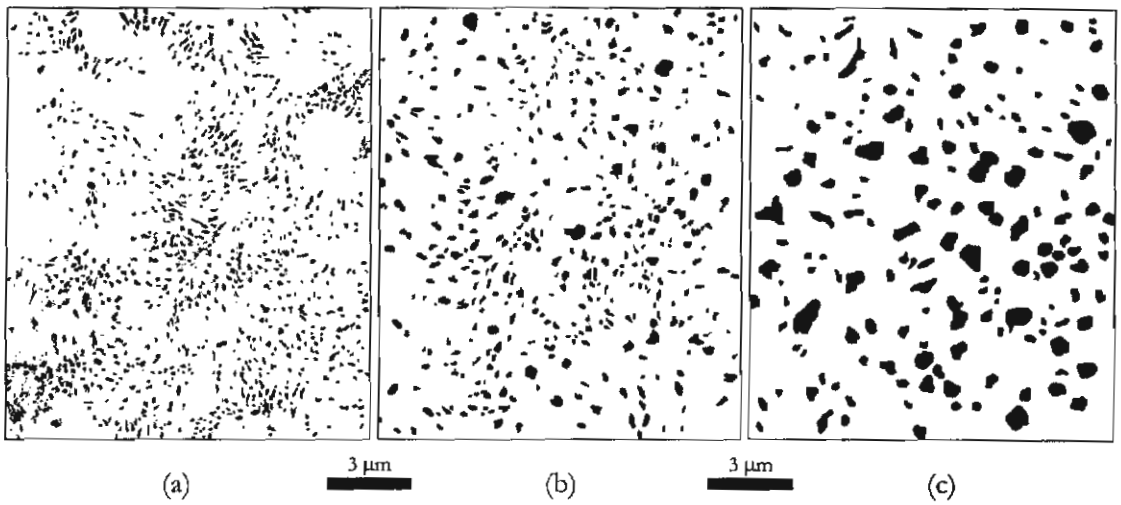

Figure 4.7 Binarised images of SEM micrographs showing the morphologies of the compression moulded impact specimens containing 10, 15, and 20 wt% EO moulded at (a), (b), and (c) 170°C.

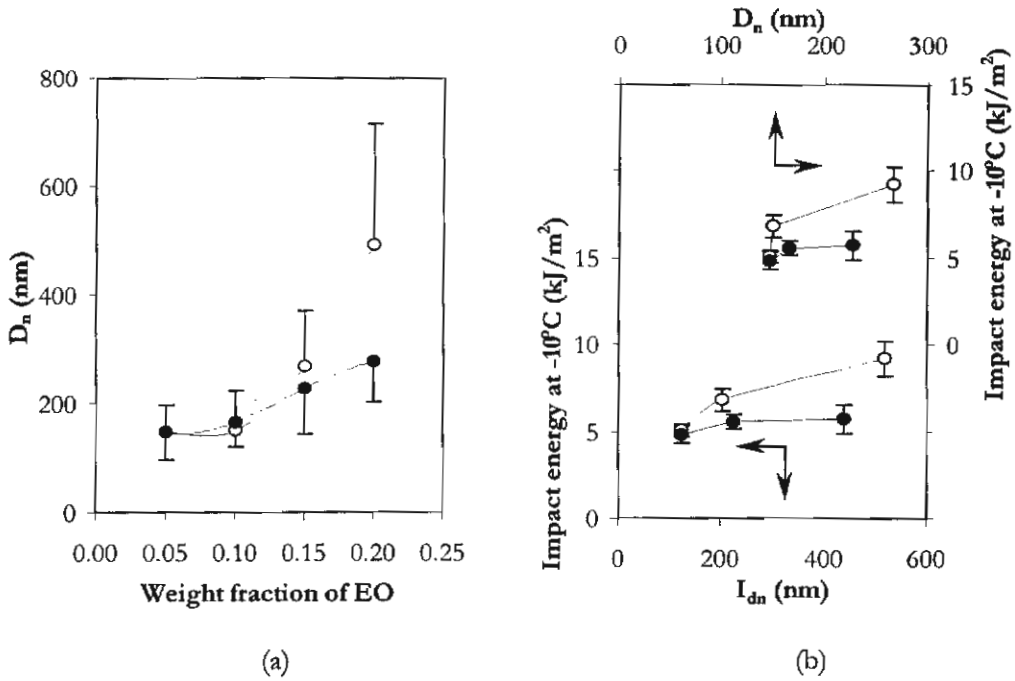

Figure 4.8 (a) Mean elastomer-rich domain diameters, D_n, in the compression moulded impact specimens moulded at (O) 170°C and (●) 230°C; error bars are the standard deviations of particle size distributions. (b) Impact energy as a function of EOC-rich mean domain diameter and average inter-particle distance.

Apparently, the very fine EOC-rich domains that are formed during quenching from microscopically homogeneous melts or near cloud point conditions are less effective at toughening the HDPE, at –10°C under Charpy impact conditions, than the coarser morphologies produced in the more strongly immiscible conditions.

CONCLUSIONS

The PE / EOC system is partially miscible in the melt state, tending towards enhanced miscibility at higher temperatures. Moreover, prior processing conditions distinctly affect the domain coarsening in subsequent processing operations, even after up to six hours annealing in the melt-state under quiescent conditions. The complex, multi-layered phase morphology produced in the solid state during moulding, is the product of the partial miscibility in the melt state and the phase separation that takes place upon cooling and crystallisation. The resultant morphology has a marked bearing upon the toughness of the material under impact conditions at sub-ambient temperature. Coarser morphologies that are a consequence of higher elastomers contents and less compatibility of the blend components at lower temperature result in greater impact toughness at sub-ambient temperature.

REFERENCES

(1) Crist B, Hill MJ (1997) J. Polym. Sci.: B: Polym. Phys. 35: 2329.

(2) Hattam P, Gauntlett S, Mays JM, Hadjichristidis N, Young RN, Fetters LJ (1991) Macromolecules 24: 6199.

(3) Rhee J, Crist B (1991) 24: 5663.

(4) Balsara NP, Fetters LJ, Hadjichristidis N, Lohse DJ, Han CC, Graessley WW, Krishnamoorti R (1992) Macromolecules 25: 6137.

(5) Krishnamoorti R, Graessley WW, Balsara NP, Lohse DJ (1994) Macromolecules 27: 3073.

(6) Bates FS, Schultz MK, Rosedale JH, Almdal K (1992) 25: 5547.

(7) Fredrickson GH, Liu AJ (1995) J. Polym. Sci.: B: Polym. Phys. 33: 1203.

(8) Hill MJ, Barham PJ, Keller A (1992) 33(12): 2530.

(9) Mader D, Thomann Y, Suhm J, Mulhaupt R (1999) J. Appl. Polym. Sci. 74: 838.

(10) Otsuka N, Yang Y., Saito H, Inoue T, Takemura Y (1998) 39(8-9): 1533.

(11) Lee CH, Saito H, Inoue T (1995) 28: 8096.

(12) Takagi S, Saito H, Chiba T, Inoue T, Takemura Y (1998) 39(8-9): 1643.

(13) Bicerano J in 'Prediction of polymer properties' (1993) Marcel Dekker, New York: 66.

(14) Dupont-Dow Elastomers (1996) Product EG 8150 data sheet.

(15) Olley RH, Basset DC (1982) Polym. Comm. 23: 1707.

(16) Cornelia V, Seymour RB in 'Handbook of polyolefins synthesis and properties' (1993) Marcel Dekker, New York.

Results Part 5

Plane stress fracture toughness of partially miscible high-density polyethylene / poly(ethylene-co-α-olefin) blends

Abstract

Blends of high-density polyethylene (PE) with poly(ethylene-co-1-octene) (EOC) were found to be partially miscible in the melt-state. Rapid crystallisation of the sheared melts led to the formation of a physically interpenetrating solid-state morphology comprising PE lamellar crystals and EOC-rich regions. Samples were extruded through a coat-hanger die at 170°C to produce anisotropic specimens for fracture toughness testing under plane stress conditions. Crystallinity and crystal size of the PE, determined through differential scanning calorimetry, were not significantly affected by the presence of the copolymer. X-ray analysis showed that there was a preferred crystal orientation that was the result of crystallisation of the oriented PE melt; moreover, a bimodal crystal orientation was observed in the pure PE compounds. The level of bimodality was reduced with increasing concentration of copolymer in the blends. For the sheet extrusion material, plane-stress fracture toughness tests revealed that the presence of the branched copolymer in the blends did not affect the work of fracture when crack propagation took place in the transverse direction of the extruded sheet, in comparison with the pure PE. The branched copolymer increased the total work of fracture for crack propagation in the machine direction due to an increase in the non-essential work of fracture, whilst in the machine direction the essential work of fracture was little altered.

INTRODUCTION

The miscibilities of polyolefin blends are strongly affected by the extents of short and long chain branching in each polymer. The solid-state morphology affects the mechanical properties, especially the toughness. Melt processing profoundly affects the morphology of polymer blends, particularly when the polymers approach the limits of miscibility. Flow enhanced miscibility has been observed in polyolefin blends under injection moulding conditions. The mechanical properties are therefore a consequence of the interaction between the polymer compatibility and the processing conditions.

In this work, the relationships between polymer compatibility in the melt state and its influence upon the solid-state morphologies and fracture toughness of a polyethylene (PE) /

poly(ethylene-co-1-octene) (EOC) system are described. Toughness determinations were carried out using a fracture mechanics approach since this permits characterisation of the mechanical deformation of the material independent of the specimen geometry. Conventional impact tests given overall energy absorption under undefined stress and strain-states. Fracture under plane stress was chosen since this condition is approximated most commonly in plastics products where the material is employed in thin sections, such as moulded part walls, films, or sheets. Plane strain conditions are only found in very thick sections and are rarely encountered, as few thick products are produced. Polyolefins are not used in thick sections due to shrinkage problems associated different rates of crystallisation through the product wall.

EXPERIMENTAL

The PE had a melt flow index of 14 g/10min, weight average molecular weight, M_w, 48,000 g/mol, and nominal density 0.962 g/cc. The copolymer used, EOC, had a melt flow index of 0.5 g/10min, M_w = 162,700, M_w/M_n = 2, and density 0.868 g/cc; it contained 7 mol% octene.

PE / EOC blends, containing 0, 5, and 10 vol% of EOC, were prepared with a Prism 16 mm twin screw extruder at a barrel temperature in all zones of 170°C and screw speed of 175 rpm. Sheets, nominally 400 μm in thickness, were prepared using a Collin 35 mm single screw extruder fitted with a coat-hanger die. The temperature profile was 170°C, die, 170°C, adapter, and 170, 170, 165, and 145°C in barrel zones 4 to 1, respectively. Barrel zones were cooled with blown air. The screw speed was 90 rpm and the chill roller, set at 50°C, was operated at 4.4 rpm.

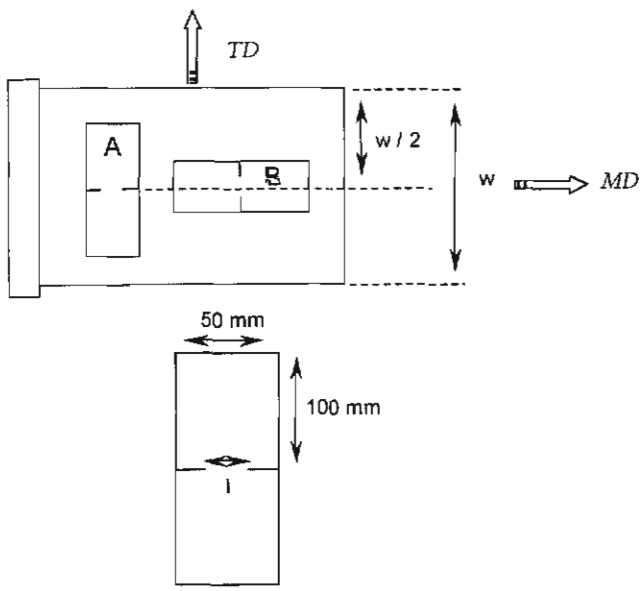

Figure 5.1 Fracture toughness specimens from the sheet extrusion material; A and B are the fracture toughness specimens, l is the ligament length, and w is the sheet width

Double edge notched specimens (length 200 mm and width 50 mm) were prepared from the sheets for fracture toughness testing as shown in figure 5.1, where TD and MD refer to the transverse and the machine direction, respectively. Results from tests upon these specimens will be referred to by the direction of travel of the crack propagation. That is, for specimen type-A the crack propagates in the machine direction; with specimen type-B, the crack propagates in the transverse direction.

The fracture toughness tests were conducted at room temperature (nominally 25°C) using an Instron 4301 tensile tester at an extension rate of 5 mm/min. All samples were notched using a razor at both sides of the sample in the centre of sample length). The notches were made perpendicular to the tensile direction, obtaining 20 specimens of each sample set with ligament lengths in the range 15 to 23 mm. Load-displacement curves were recorded and the absorbed energy was calculated from the weight of load-displacement papers. Tensile tests were carried out using an Instron 4301 tensile tester at an extension rate of 5 mm/*min* upon dumbbell samples punch in the MD and TD of the sheet.

Sections for transmission electron microscope observation (TEM), obtained using an RMT ultramicrotome, were stained with ruthenium tetraoxide vapours. Permanganic acid etched surfaces of the stubs remaining from the samples after sectioning were viewed using a scanning electron microscope (SEM) after vapour deposition of a platinum-palladium alloy.

X-ray analysis

Wide-angle X-ray diffraction measurements were made by using nickel-filtered CuK_α radiation using a Bruker powder X-ray diffractometer (model D8 advance) operated at 40 kV and 40 mA. All scans were recorded with transmission technique. The azimuthal scans of (200) and (020) plane reflections (diffraction angle $°2\theta$ = 23.9 and 36.3°, respectively) for poly(ethylene-co-1-octene) and polyethylene blends were carried out at a scan speed of $3°min^{-1}$.

RESULTS AND DISCUSSION

Figure 5.2 shows TEM micrographs displaying typical solid-state morphologies of the pure PE and a PE / EOC blend, both processed at 170°C. As was discussed in part one of this report, the white lines are PE lamellae of around 17 nm thick.

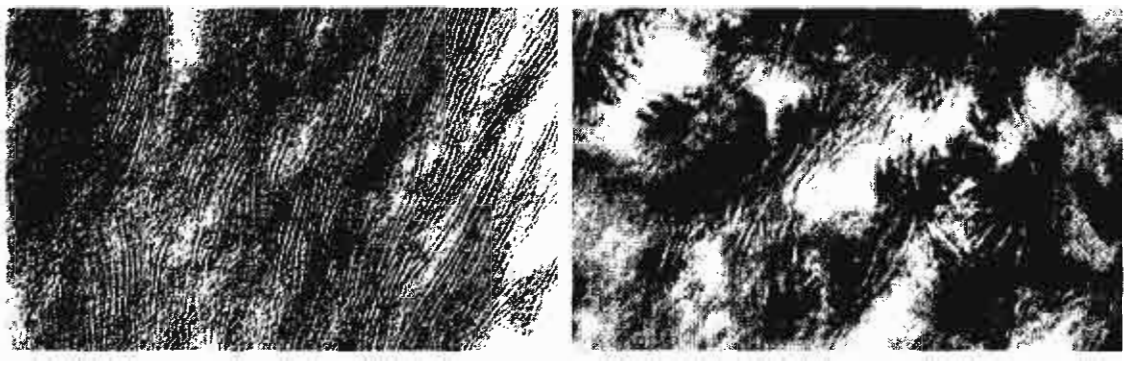

(a) (b)

Figure 5.2 TEM micrographs of (a) pure PE and (b) a PE / EOC blend melt-processed at 170°C

The dark areas are the EOC-rich regions. It can be seen that the PE crystals penetrate into the EOC-rich regions. From this observation, it was inferred that at least some of the PE and the EOC were mixed in the melt-phase at the time of crystallisation. As explained in a previous publication [1], and part one of this report, thermal analysis revealed that in the solid state the material comprised essentially pure domains of amorphous EOC and amorphous PE, since there were no significant differences between the glass transition temperatures of the components in the pure materials and the corresponding transitions in the blend samples.

Orientation

The orientation function f describes the orientation of the crystalline axis relative to some reference direction in the sample. The orientation function is defined as

$$f_x = \frac{3\overline{\cos^2 x} - 1}{2} \qquad (1)$$

where $\overline{\cos^2 x}$ designates the average cosine squared value of the angle x between the reference direction in the sample and the x crystallographic direction.

Stein [1] has set up a generalized model for uniaxial crystal orientation of polyethylene unit cell in the coordinate system as shown in figure 5.3.

The Z axis of the X, Y, Z cartesian coordinate system is taken as the stretching direction. The angles α, β, and ε are measured between the Z Axis and the a, b, and c crystallographic axes, respectively.

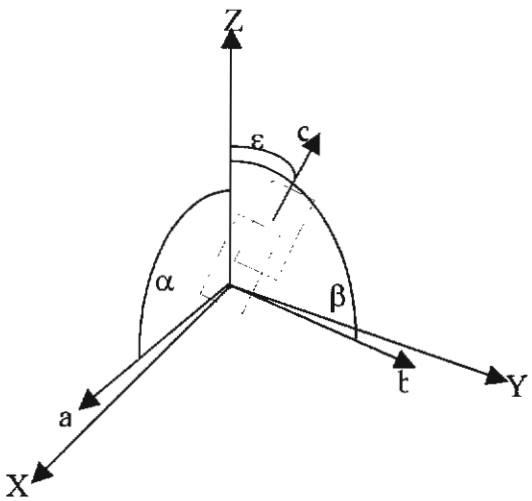

Figure 5.3 The coordinate system used for describing the orientation of polyethylene crystal

Since the three axes are perpendicular for the orthorhombic unit cell,

$$\overline{\cos^2\alpha} + \overline{\cos^2\beta} + \overline{\cos^2\varepsilon} = 1 \tag{2}$$

and therefore

$$f_\alpha + f_\beta + f_\varepsilon = 0 \tag{3}$$

where the three orientation functions are defined as:

$$f_\alpha = \frac{3\overline{\cos^2\alpha} - 1}{2} \tag{4}$$

$$f_\beta = \frac{3\overline{\cos^2\beta} - 1}{2} \tag{5}$$

$$f_\varepsilon = \frac{3\overline{\cos^2\varepsilon} - 1}{2} \tag{6}$$

Thus for this model, the three orientation functions are not independent and only two of them are required to characterize the orientation.

Crystalline orientation was determined by the measured intensity I_{meas} in counts per second at each azimuthal angle, ψ, where the azimuthal angle is defined as the angle between the stretching direction and the plane of measurement of θ_{hkl}. The measured intensity must be corrected for absorption [2], polarization and background before it can be used to evaluate $\overline{\cos^2\phi_{hkl}}$. The equation used for correction of the measured intensity is

$$I(\psi) = (I_{meas} - I_{background})K_{polarization}\, K_{absorption} \tag{7}$$

Where $I_{background}$ is background intensity

$$K_{polarization} = \frac{2}{1+\cos^2(2\theta_{hkl})} \tag{8}$$

$$K_{absorption} = \frac{\mu t(\sec 2\theta_{hkl} - 1)}{1-\exp[-\mu t(\sec 2\theta_{hkl} - 1)]} \tag{9}$$

where μ is the linear absorption coefficient and t is the thickness of the sample film. For a system that is oriented uniaxially,

$$\overline{\cos^2\psi_{hkl}} = \frac{\int_0^{90} I(\psi)\cos^2\psi \sin\psi d\psi}{\int_0^{90} I(\psi)\sin\psi d\psi} \tag{10}$$

Equation (10) can be used to evaluate by multiplying the corrected intensities by the appropiate values of the sine and cosine function and plotting the results against the azimuthal angle. The area under the curves can be calculated by numerical integration by method of trapezium rule. Azimuthal scans for the (200) and (020) crystal plane of the orthorhombic PE crystals are displayed in figure 5.4. The DSC and X-ray values calculated for the PE samples are listed in table 1.

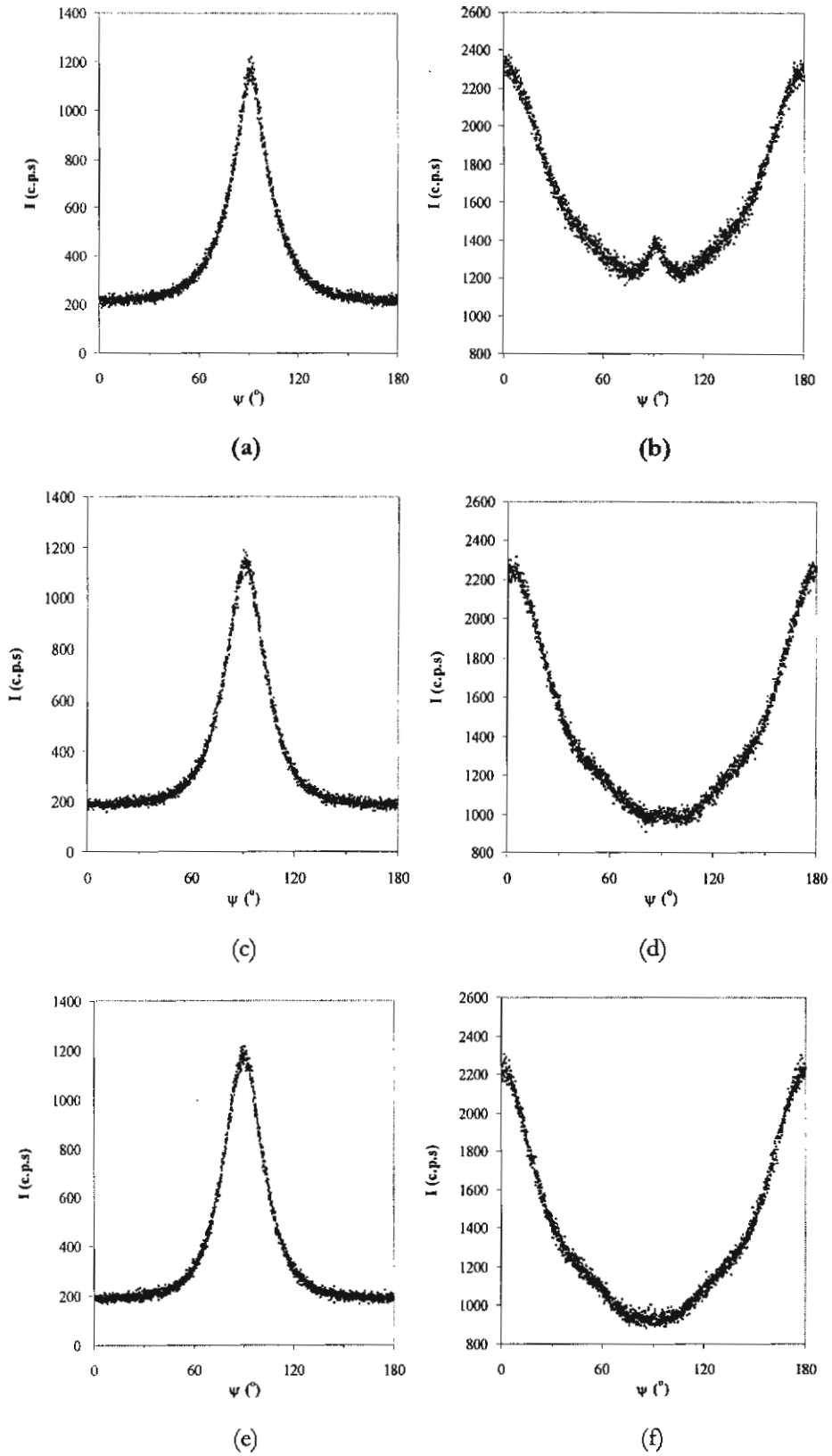

Figure 5.4 Azimuthal angle scans for specimens in reflection mode: (a) PE (020) plane, (b) PE (200), (c) 5 vol% EOC (020) plane, (d) 5 vol% EOC (200), (e) 10 vol% EOC (020) plane, and (f) 10 vol% EOC (200) vol%.

Table 1. Orientation from X-ray data, peak melting point, Tm, and crystallinity, C, from DSC for the sheet extrusion PE compounds*

EOC content (vol%)	f_α	f_β	f_ε	C (vol%)	Tm (°C)
0	0.067	-0.211	0.143	58.0	133.6
	(0.007)	(0.007)	(0.016)	(0.70)	(0.14)
5	0.100	-0.234	0.135	57.2	133.9
	(0.004)	(0.006)	(0.010)	(1.27)	(1.60)
10	0.096	-0.237	0.141	57.4	133.5
	(0.004)	(0.002)	(0.002)	(1.54)	(0.89)

* numbers in parenthesis are the standard deviations from three replicate determinations

Melting temperature and heat of fusion data reveal that the presence of the copolymer in the blends did not significantly affect the crystal size or crystallinity, respectively. The X-ray analysis characterises the preferred crystal orientation of the PE crystals that arises due to crystallisation of the PE melt, oriented principally uniaxially by the flow through the coat hanger die and subsequent haul-off. The Azimuthal scan of the (200) plane of the pure PE indicates a bimodal crystal orientation, as evidenced by the increase in scattering intensity in the ± 20° range centred at 90°, Ψ. This may be a consequence of the row-nucleation mechanism whereby crystals form perpendicular to one another. The precise mechanism of formation is not agreed upon at present, but is thought to be caused by a second population of crystals being nucleated around the regions of the initial crystal formation. The rise in intensity at 90°, Ψ, is less pronounced in the samples containing EOC. Moreover, the effect lessens as the content of EOC increases. Apparently, the presence of EOC in the extruded samples interferes with the row-nucleation process, and hence suppresses the formation of the second population of crystals perpendicular to the first.

Fracture studies

The fracture toughness of the materials was studied using the essential work of fracture method. This method was based on the assumption that [2]

$$w_f = w_e + \beta w_p l$$

where β is the shape factor, l is the ligament length and w_f, w_e, and w_p are the specific total, essential, and non-essential work of fracture, respectively. A linear plot of w_f versus l was used to determine w_e and βw_p under plane stress conditions.

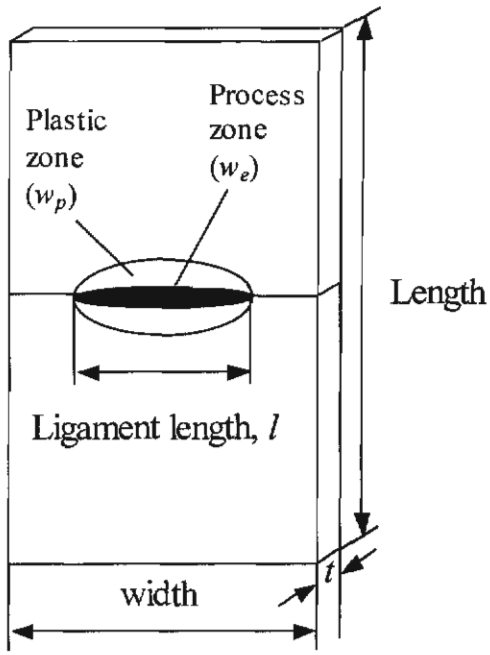

Figure 5.5 The DENT samples used for the essential work of fracture test.

The intercept of the plot is the essential work of fracture. That is when the least sum of squares fit to the experimental data is extrapolated to zero ligament length. Linearity of the plot is associated with plane stress conditions. The slope of the plot is related to the non-essential work of fracture. As illustrated in figure 5.5, this analysis allows characterisation of the energy absorbed in the 'process zone' involved with the cracking process and the 'plastic zone' that surrounds the process zone, rather than giving an ill-defined overall energy consumption value.

Figure 5.6 and 5.7 show plots of specific fracture energy versus ligament length for the specimens in which the crack propagated in TD and MD, respectively. The linearity of the plots indicates that the samples tested were deformed under plane stress conditions over the range of ligament lengths that was employed.

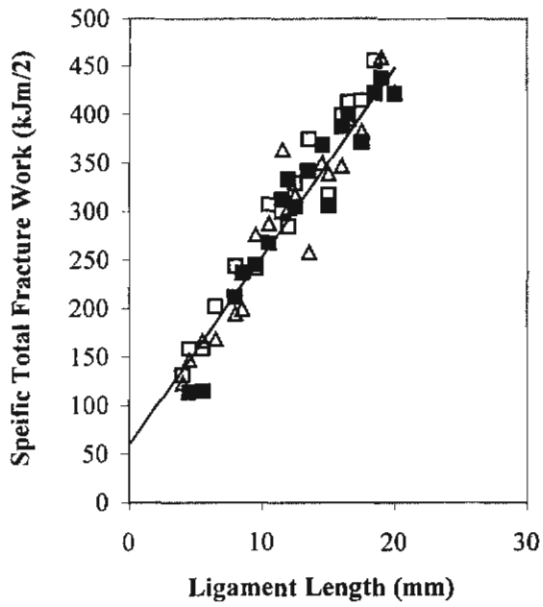

Figure 5.6 Crack propagation in TD: (□) PE pure, (■) PE / EOC 5vol%, and (Δ) PE / EOC 10vol%

Data for the analysis of fracture of sheet samples, obtained from the gradients of the plots and the energy-axis intercepts, are documented in table 2. The plane stress fracture toughness for crack propagation in the MD was strongly influenced by EOC content while for crack propagation in the TD, EOC had no influence.

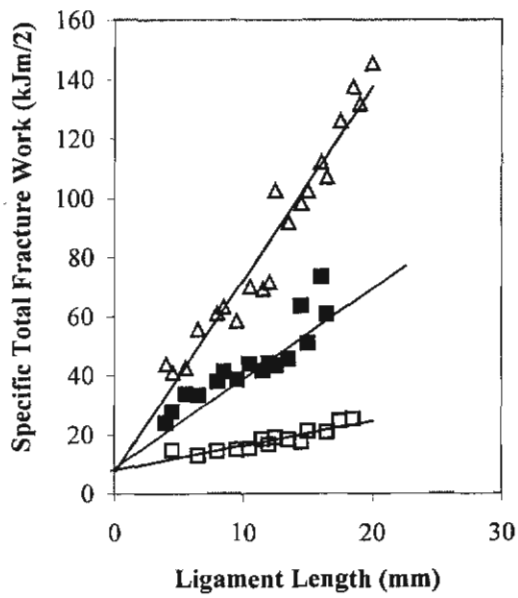

Figure 5.7 Crack propagation in MD: (□) PE pure, (■) PE / EOC 5vol%, and (Δ) PE / EOC 10 vol%

Specifically, the presence of partially miscible EOC affected the non-essential work of fracture *(w_p)* while the essential work of fracture *(w_e)* was little affected by EOC when the crack propagated in the MD.

Table 2. Tensile test and plane stress fracture toughness data obtained from extruded sheets for crack propagation in the machine direction (MD) and transverse direction (TD)*

EOC content (vol%)	Crack propagation direction	Tensile strength+ (MPa)	Breaking strain+ (%)	We (kJm^{-2})	βw_e (kJm^{-2})
0	MD	12.8	305	7.9	0.9
		(1.05)	(78)		
	TD	26.2	344	59.2	20.9
		(0.85)	(39)		
5	MD	12.4	379	8.3	2.4
		(1.97)	(78)		
	TD	28.1	275	46.2	20.5
		(0.85)	(19)		
10	MD	12.9	407	7.4	5.6
		(3.05)	(69)		
	TD	27	284	59.5	19.4
		(0.59)	(21)		

* numbers in parenthesis are the standard deviations from ten replicate determinations

\+ note the tensile data relevant for the crack propagation in MD is from the samples tensile tested in TD and vice versa for crack propagation in the TD

The orientation of the PE in the MD dominated the crack processes travelling in the TD. This was related to higher tensile strength in the MD, as shown in table 2, which was a consequence of the orientation process, with the tensile strength in the direction of orientation being around double that in the perpendicular direction. This is because the energy absorbed, i.e. the fracture toughness, is the product of the tensile force and the sample extension. However, the orientation led to enhanced crack propagation in the MD, associated with reduced tensile strength in the transverse direction. The presence of the interlocked EOC-rich and PE domains resulted in greater energy dissipation through the non-essential work of fracture.

CONCLUSIONS

The presence of the branched copolymer affected the fracture of PE differently depending upon the state of the test specimens. For crack propagation in the TD, the orientation of the PE dominated the fracture process and hence the presence of EOC had little effect. For crack propagation in the MD, the branched copolymer increased the non-essential work of fracture, but had little effect upon the essential work of fracture.

REFERENCES

1. A. Tabtiang, B. Parchana, R. A. Venables, and T. Inoue, *J. Polym. Sci.: Part B: Polym. Phys.*, **39**(3), (2001)

2. J. Wu and Y. W. Mai, *Polym. Eng. Sci.*, **36**, 2275 (1996)

3. R. S. Stein, J. Polym. Sci., **31**, 327 (1958)

4. R. J. Samuels, *Structured Polymer Properties: The Identification, Interpretation, and Application of crystalline Polymer Structure;* Wiley-Interscience: New York (1974)

5. L.E. Alexander, *X-Ray Diffraction Methods in Polymer Science;* Wiley-Interscience: New York (1969)

Conclusions

The thermomechanical history of polyolefin blends has a pronounced effect upon the morphology development, and therefore the physical properties of the materials. The effects of temperature and shear history differ depending upon the inherent mutual compatibility of the constituent polymers.

In systems that were deemed partially miscible, such as the polyethylene / poly(ethylene-co-1-octene) blend, melt flow resulted in the formation of a fine length-scale morphology comprising intertwined polyethylene lamellae and poly(ethylene-co-1-octene) domains. The morphology resulted from the concurrent liquid-liquid and solid-liquid phase separation that occurred upon cessation of flow and cooling.

In the partially miscible systems, shearing was found to affect the superposition of time and temperature upon the coarsening process that was observed for samples prepared without shearing. Shearing two-phase melts at 1 s^{-1} led to coarsening of the domain morphology at an accelerated rate in comparison with unsheared samples and those sheared at 50 s^{-1}. In all cases, conditioning of samples at elevated temperature resulted in reduced coarsening during subsequent annealing. Moreover, the influence of elevated temperature was enhanced through intensive shearing during injection moulding. The short time spent at the elevated temperature has a critical effect upon the morphology that forms in subsequent operations. This effect was not a consequence of changes in melt viscosity, as evidenced by the non-superimposition of the results data when the superposition of time and temperature was assumed. The complex, multi-layered phase morphology produced in the solid state during moulding, was the product of the partial miscibility in the melt state and the phase separation that takes place upon cooling and crystallisation. The resultant morphology has a marked bearing upon the toughness of the material under impact conditions at sub-ambient temperature. Coarser morphologies that are a consequence of higher elastomers contents and less compatibility of the blend components at lower temperature result in greater impact toughness at sub-ambient temperature.

In the isotactic polypropylene and isotactic poly(propylene-co-ethylene) systems that exhibited poorer compatibility than the polyethylene formulations, the impact properties were critically dependent upon the injection molding conditions, with decreases in toughness associated with increased elastomer domain sizes at higher molding temperatures. For the PE that exhibited pronounced miscibility in the melt-state, differences in the processing conditions had a relatively minor influence upon impact toughness.

The presence of the branched copolymer affected the fracture of PE differently depending upon the state of the test specimens. For crack propagation in the TD, the orientation of the PE dominated the fracture process and hence the presence of EOC had little effect. For crack propagation in the MD, the branched copolymer increased the non-essential work of fracture, but had little effect upon the essential work of fracture.

It has been shown that the processing history has a pronounced effect upon the morphology development of polyolefin blends. The effect of shearing and temperature have a critical effect upon the morphology that forms through subsequent processes, in some cases resulting in a 200 to 300 % difference in measured toughness. Moreover, the key findings are that it is vital to understand the mechanism of morphology development since this has an important effect upon the morphology that is subsequently produced. This has particular relevance in polymer processing because polymer materials usually experience two to three stages of melt processing in the production of a finished article. Each step of the processing then must be considered to understand the morphology and properties of the finished article.

Output:

Two published manuscripts:

Tabtiang T, Parchana B, Venables RA, Inoue T. *'Melt Flow Induced Phase Morphologies of a High-Density Polyethylene/Poly(ethylene-co-1-octene) blend'.* ***J. Polym. Sci.: Part B: Polym. Phys.***, 39(3), (2001)

Tabtiang T, Parchana B, Venables RA, *'The relationship between processing history and the morphology of injection moulded toughened polyolefins'. Polym.-Plast. Technol. Eng.*, 40(4), pp.423-436 (2001)

Three papers in preparation.

Two Ph.D. theses

One M.Sc. thesis

Nine undergraduate final year projects

POLYM.–PLAST. TECHNOL. ENG., 40(4), 423–436 (2001)

THE RELATIONSHIP BETWEEN PROCESSING HISTORY AND THE MORPHOLOGY OF INJECTION MOLDED TOUGHENED POLYOLEFINS

A. Tabtiang, B. Parchana, and R. A. Venables*

Department of Chemistry, Faculty of Science, Mahidol University, Rama VI Road, Bangkok 10400, Thailand

ABSTRACT

The solid-state morphologies of three polyolefins, namely isotactic polypropylene (iPP), isotactic poly(propylene-co-ethylene) (iPcE), and high-density polyethylene (PE), toughened with an elastomeric poly(ethylene-co-1-octene) (EcO) have been investigated. Morphologies ranged from dispersed droplets with mean diameters in the range 0.2 to 0.6 μm, for iPP, to a fine interpenetrating morphology comprising 17 nm thick lamella crystals and elastomer-rich regions of length-scale 170 nm when the major component was linear PE. In the iPcE formulations, 10 nm thick lamellar crystals of the matrix polymer were observed in the elastomer domains. Dynamic mechanical analysis and microscopy of quenched and annealed samples showed that each system was phase separated in the solid state and in the melt under quiescent conditions, respectively. The differing solid state morphologies

*Corresponding author. Fax: 662-247-7050; E-mail: frrav@mahidol.ac.th

were inferred to result from the mixing under melt flow of the partially miscible polymers during processing and by the subsequent liquid–liquid and solid–liquid phase separation on cooling.

Key Words: Toughened polyolefins; Morphology; Partial miscibility

INTRODUCTION

The toughness of plastics modified with a minority elastomer component is critically dependent on the domain size and morphology of the dispersed phase (1). These factors are influenced by the extent of miscibility of the constituent polymers and the melt processing conditions. Melt stresses and processing time affect the dispersion and coalescence processes; moreover, when the blend components approach the limits of miscibility, the extent of mixing at the molecular level may be affected. The work of Madbouly et al. (2) has shown that flow affects the thermodynamics of miscibility: It was determined that melt flow effected a shift in the glass transition temperatures of polystyrene/poly(vinyl methyl ether) blends in comparison with the same materials that were biphasic at the equal temperature under quiescent conditions. The results were interpreted as an upward shift of the lower critical solution temperature. In the case of polyolefin blends, the heat of mixing is small, and hence the entropy of mixing is relatively important, in comparison with blends that have enhanced miscibility due to specific interactions. Melt flow may be expected to alter the entropy of the system thereby affecting the mixing (3,4).

In this work, the influence of processing history on the solid-state morphologies of several injection molded polyolefins containing poly (ethylene-co-1-octene) as the minority elastomer phase has been investigated. Evidence for mixing at the molecular level under melt flow is presented.

EXPERIMENTAL

Details of the polymer resins used in this work are shown in Table 1; MFI is melt flow index, and M_w, M_n, and M_z are the weight, number, and z-average molecular weights, respectively, determined using a Waters gel permeation chromatograph employing polystyrene standards in trichlorobenzene solution at 145°C. $N_w = M_w/M_0$; i.e., the weight average degree of polymerization and M_0 is the relative molecular mass of the polymer repeat unit. The EcO was compounded with each of the iPP, iPcE, or PE resins, in various weight ratios, using a Prism 16 mm twin screw extruder at a barrel temperature of 180°C and screw speed of 175 rpm. Injection moldings were prepared using a Dr Boy 22S machine, employing barrel temperatures between 170 and 230°C; the mould temperature was 30°C. Plasticization energy, that is the mechanical work applied through the

Table 1. Resin Characteristics

Polymer Resin	Code	Comonomer, (mol%)	Density, (g cm^{-3})	M_w, (g mol^{-1})	N_w	M_z, (g mol^{-1})	M_w/M_n	MFI (dg min^{-1})
iPoly(propylene-co-ethylene)	iPcE	5	0.900	214,000	2240	407,000	3.4	12[a]
Poly(ethylene-co-1-octene)-1	EcO1	25	0.868	172,000	3506	283,000	2.2	5[b]
Poly(ethylene-co-1-octene)-2	EcO2	25	0.868	261,000	5320	389,000	2.1	0.5[b]
iPolypropylene	iPP	0	0.905	291,000	3725	475,000	2.9	10[a]
Polyethylene-1	PE1	0	0.962	128,000[c]	4563	—	—	18[b]
Polyethylene-2	PE2	0	0.962	155,000	5525	396,000	3.7	14[b]

[a]BS 720A Test condition 12.
[b]BS 720A Test condition 4.
[c]Datum from correlation of MFI with resins of known molecular weight.
MFI is melt flow index; M_w, M_n, and M_z are weight, number, and z-average molecular weights, respectively; N_w is weight average degree of polymerization; Prefix 'i' in iPP and iPcE denotes isotactic.

screw was adjusted through control of the back-pressure, in the range 0 to 1.7 MPa, and screw speed, in the range 50 to 150 rpm. Small batches (60 g) were also prepared using a Haake Rheocord 90-torque rheometer at 170°C and 50 rpm for 5 min. These samples were used for shearing using a custom-built parallel plate apparatus where the plates could be rapidly demounted such that quenching of the sample in cold water could be carried out.

Shear flow data were generated using a Rosand capillary rheometer and a Haake RT20 parallel-plate rheometer. Charpy impact data were collected using a Zwick pendulum impact tester; specimens were chilled to −10°C in a water/ethylene glycol solution that was cooled using a Neslab RTE111 liquid recirculator or to 0°C in an ice/water slush. Blends of varying composition were annealed in an oil bath, after wrapping in aluminum foil, for 6 h at temperatures in the range 140 to 270°C. For higher temperatures the specimens were heated in a tube furnace under nitrogen flow. A thermocouple was inserted in the sample to monitor its temperature. Transmission electron micrographs (TEM) were obtained from RuO_4 vapor stained sections. Unstained sections were viewed with a Nikon E400 transmitted light microscope; the fraction of hexagonal crystals in the iPP samples was determined from the area fraction of highly birefringent spherulites viewed through crossed-polarizing filters. Flat surfaces, prepared with a microtome at −100°C, were treated with a permanganic acid reagent (0.7 w/v% solution at 30°C) (5), to selectively etch the amorphous material, or with toluene at 30°C and viewed using a scanning electron microscope (SEM) after coating with metal. Scanned and calibrated micrographs were quantitatively analyzed using ImagePro software to obtain lamella thickness, area fractions, and mean dispersed domain diameters. All microscopy data presented herein refer to the cores of the samples. Differential scanning calorimeter (DSC) data were obtained with a Perkin Elmer DSC7 instrument: specimens (10 mg ± 0.1 mg) were cut from the central core of the moldings and dipped in silicone to ensure rapid heat transfer to the specimens. Fusion endotherms were obtained at a heating rate of 30°C/min, to limit annealing during heating, under a nitrogen atmosphere. Wide angle X-ray diffraction patterns were collected with a JEOL JDX-350 instrument. Dynamic mechanical analyses were carried out using a Polymer Laboratories DMTA mkII instrument in tensile mode at a deformation frequency of 10 Hz and heating rate of 5°C/min.

RESULTS AND DISCUSSION

Isotactic Polypropylene Homopolymer Formulations

The Charpy impact properties, at 0°C, of the PP/EcO2 (70:30 w/w) compounds, injection molded under various conditions are illustrated in Figures 1 and 2 as functions of mean dispersed phase diameter (determined from micrographs of

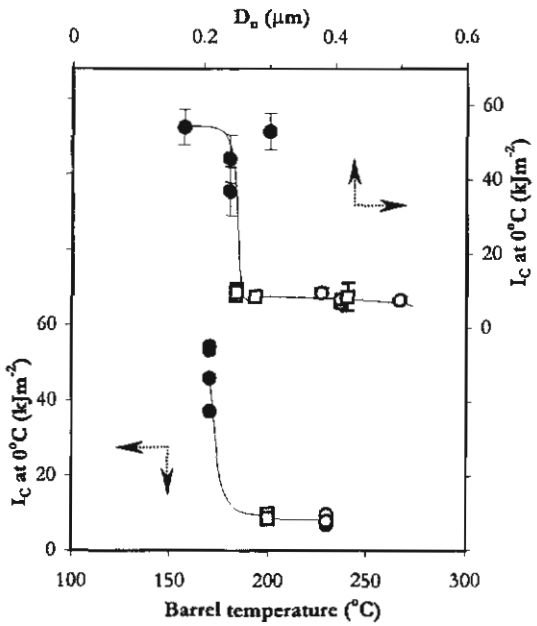

Figure 1. Charpy impact energies, I_C, at 0°C of toughened PP samples containing 30 wt% EcO2. Data are plotted versus mean elastomer domain size and barrel temperature for samples molded at (•) 170°C, (□) 200°C, and (○) 230°C. Error bars are ± the sample standard deviation.

solvent-etched microtomed surfaces), barrel temperature, and specific mechanical energy input, S_e. The power dissipated per unit volume during plasticization, P, was taken as (6)

$$P = \eta(\dot{\gamma})^2,$$

where η is the viscosity at shear rate, $\dot{\gamma}$. Shear rate in the channel of screw metering zone was estimated (7) as

$$\dot{\gamma} = \frac{\pi D N}{h},$$

where D is the screw diameter, N the screw speed, and h the screw channel depth. S_e was calculated as

$$S_e = Pt,$$

where t is the plasticization time. The impact energies are critically dependent on the domain size of the elastomer inclusions; a mean domain size of 0.3 μm separates low and high toughness groups of samples. This effect in semicrystalline

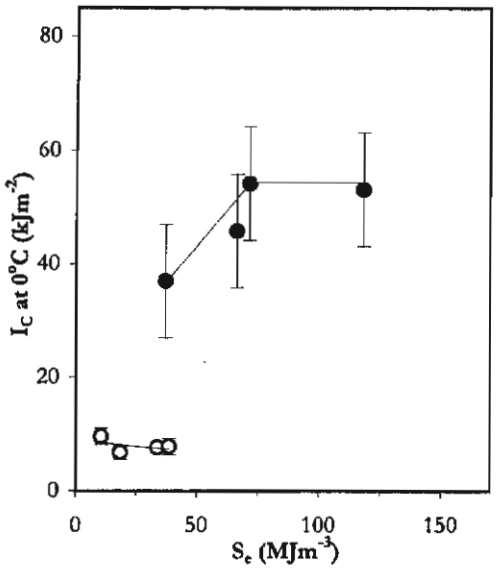

Figure 2. Charpy impact energies, I_C, at 0°C of toughened PP samples containing 30 wt% EcO2. Data plotted as a function of plasticization energy, S_e, during injection molding at barrel temperatures of (•) 170°C and (○) 230°C.

plastics has been explained in terms of a critical inter-particle distance (or ligament length), I_d, that is a function of the volume fraction of the dispersed domains, ϕ_d, domain size, D_n, and packing geometry (8)

$$I_d = D_n \left[\left(\frac{\pi}{6\phi_d} \right)^{1/3} - 1 \right].$$

The model assumes simple cubic packing, and hence the ligament lengths for the molded samples are in the range 35 to 86 nm with a critical value of 61 nm. The mean domain size in the extruded compound, i.e., prior to injection molding, was 0.29 μm. Moldings prepared using the higher barrel temperatures had lower impact toughness, due to the presence of larger elastomer domains, and hence increased ligament lengths. This was presumably due to the enhanced rate of interfacial tension driven droplet coalescence associated with the lower viscosity conditions encountered at high temperature. Plasticization energy had little effect on the toughness of samples prepared at 230°C, most likely due to the dominance of coalescence at this temperature. Higher plasticization energies, achieved through increasing back pressure and screw speed, when the barrel temperature was 170°C led to enhanced impact toughness. The latter effect may be largely traced to the influence on domain size with the increased melt stresses

counteracting the coalescence. It was determined through polarized light microscopy that typically the cores of the iPP moldings comprised spherulites of around 10 μm in diameter, 18.0 area% of which were made of the hexagonal and 82.0 area% of monoclinic crystal type. The presence of the hexagonal form was confirmed through X-ray diffractometry; the triclinic form was absent. The average crystallinity, $\%\chi$, through DSC analysis, of all iPP samples prepared was 44.1 wt% from

$$\%\chi = \Delta H_f \left(\frac{w_{f(\alpha)}}{\Delta H_{(100\alpha)}} + \frac{w_{f(\beta)}}{\Delta H_{(100\beta)}} \right) 100,$$

with a coefficient of variation (CV = standard deviation/mean) of 4.3%; $w_{f(\alpha)}$ and $w_f(\beta)$ are the fraction of monoclinic and hexagonal spherulites. The heat of fusion for a 100% crystalline iPP in monoclinic form, $\Delta H_{(100\alpha)}$, was 207 J/g (9), and the corresponding value for the hexagonal form, $\Delta H_{(100\beta)}$, was 113 J/g (10). CV from replicate samples prepared at 200°C was 2.3%. The average peak melting temperature of all iPP samples, by DSC, was 164°C with a CV of 0.3%; replicate analyses gave a CV for experimental error as 0.2%. Moreover, Scherrer crystallite size, L_S, calculations from (11) $L_s = \lambda/(\beta_{hkl} \cos\theta)$ were qualitatively consistent with the melting data; where λ is the wavelength of the X-ray radiation, β_{hkl} is the peak width at half maximum intensity, in radians, of the hkl reflection in the WAXD patterns, and θ is the diffraction angle. Thus, the crystal characteristics of the iPP were little sensitive to the presence of elastomer or the molding conditions employed, in comparison with experimental error. The toughened iPP sample behaves as a compatible mixture with no evidence of mixing of the matrix and elastomer at the molecular level. Domain size was the principal variable determining impact toughness. A typical morphology of a compound with an iPP matrix is shown in Figure 3.

Isotactic Poly(Propylene-co-ethylene) Compounds

In the iPcE samples containing EcO1, the elastomer inclusions have several features that were not seen in the iPP samples; this is exemplified by the TEM micrograph of an iPcE compound in Figure 4a. In Figure 4b, an image with the contrast adjusted to emphasize the lamella texture in the matrix is shown. Lamellar crystals of comparable thickness to those seen in the continuous phase; i.e., in the range 10 to 11 nm, are located in the elastomer domains. While the elastomer is partially crystalline, possessing a nominal weight fraction crystallinity of less than 0.138, it has a broad melting endotherm covering the range 40 to 60°C, by DSC. This would not be consistent with a lamellar thickness of 10 nm. The weight

Figure 3. TEM micrograph showing the detail of the morphology of a PP sample containing 40 wt% of EcO2. The sample was mixed in an internal mixer, sheared between parallel plates at 230°C, and then quenched. Micrograph shows a section taken at 5 mm from the center of the sample; at this position, shear rate was 10 s^{-1}.

fraction crystallinity, w_c, was determined:

$$\frac{1}{\rho} = \frac{w_c}{\rho_c} + \frac{(1 - w_c)}{\rho_a}$$

where ρ, ρ_c, and ρ_a are the total density, density of pure crystalline, orthorhombic, PE [1000 kg m^{-3} from X-ray analysis (12)], and the density of amorphous PE [854 kg m^{-3} from extrapolation of melt densities to 298 K(12)], respectively. Based upon the Gibbs-Thompson equation (13)

$$L_c = \frac{T_m^0 2\sigma_e}{(T_m^0 - T_m)\rho_c \Delta H^0},$$

considerably thinner crystals, with thicknesses, L_c, in the range, 2.5 to 3.1 nm, are anticipated; T_m^0 is the equilibrium melting point of linear PE from the Hoffmann-Weekes method (415 K) (12), σ_e is fold surface energy of an orthorhombic PE crystal (90 mJ m^{-2}) (12), T_m is the melting point, and ΔH^0 is the heat of fusion of an ideal orthorhombic PE crystal (293 J g^{-1}) (12). Moreover, the extensive chain branching and even branch distribution of the EcO may preclude the formation of regularly folded lamellar crystals since the elastomer possess, on average,

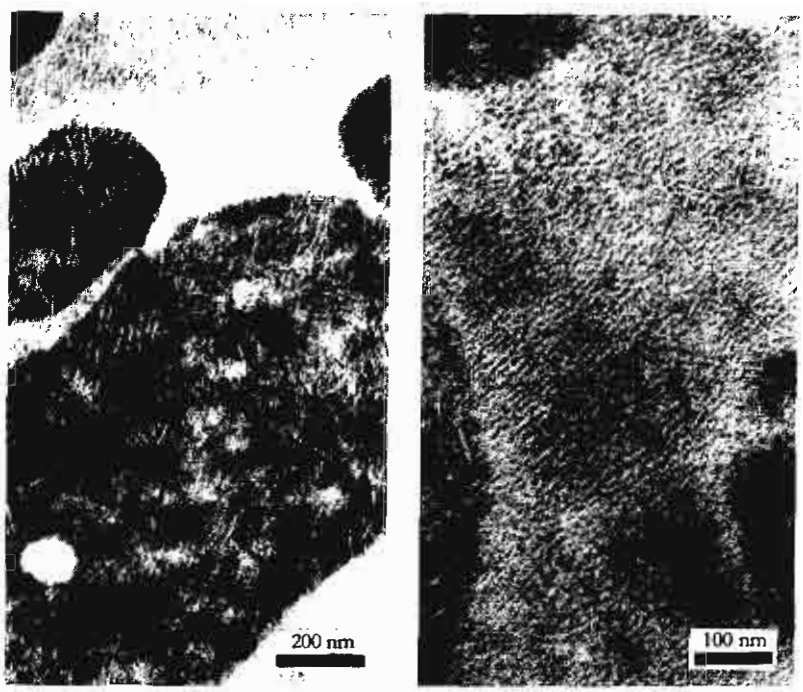

(a) (b)

Figure 4. TEM micrographs of a PcE sample containing 30 wt% EcO1 injection molded at 170°C and 0 Pa back-pressure. a) Showing lamellar crystals in the elastomer domains; the white drop in the stained domain at bottom left is thought to be mechanically occluded matrix. b) Contrast adjusted to emphasize lamella texture of the matrix.

one hexyl-branch per eight backbone carbon atoms. If $\sigma_e = 62.5$ mJ m^{-2} (14), $\rho_c = 936$ kg m^{-3} (14), $T_m^0 = 461$ K (14), and $\Delta H^0 = 207$ J g^{-1} (9) for an ideal monoclinic iPP crystal, the experimental melting point of 158°C (431 K) gives an anticipated lamellar thickness of 10 nm for the iPcE. It is therefore inferred that the lamellae in the elastomer domains comprise iPcE. The lamellae are less distinct in the matrix, because the iPcE-rich phase is less readily stained by the RuO_4 vapor although the characteristic crosshatched texture of iPP is discernable in Figure 4b. The iPcE crystals are clearly seen within the elastomer domains in Figure 4a, however, because they are lightly stained in contrast with the high concentration of highly stained EcO. It is reasonable to conclude that these lamellae were formed through the crystallization of iPcE that was dissolved in the EcO under the processing conditions. The dispersed domains in the iPcE samples containing 30 wt% (equivalent to 30.9 vol% at 298 K) of EcO injection molded at

170 and 230°C, with a back-pressure of 0 Pa, had mean domains sizes of 0.35 and 0.70 μm, respectively. Furthermore, the corresponding area fractions were 0.47 and 0.54, respectively. Thus, the area fractions are higher than would result from simple incorporation and dispersion of the elastomer into the matrix. The corresponding ligament lengths for these samples are thus 13 nm and zero. The zero value is reached due to the assumption of simple cubic packing where the maximum packing fraction is 0.52; the real system, however, with random packing and polydisperse particle sizes will have larger ligament lengths than predicted. The Charpy impact energies at 0°C of these iPcE compounds were 10.0 kJ m^{-2} and 4.7 kJ m^{-2} for the samples injected molded at 170 and 230°C, respectively. The short ligament lengths resulting from an increase in the volume fraction of the elastomer-rich domains due to the incorporation of iPcE may reduce the effectiveness of the rubber toughening and also increase the probability, and hence rate, of dispersed droplet contact and coalescence. In this work, under no conditions could a single phase melt for this blend be prepared under quiescent conditions; that is, up to 350°C under nitrogen where embrittlement of the polymers became apparent. The morphology is thus thought to be a consequence of the partial mixing of the polymers under melt-flow.

A mottled texture of light and dark areas is seen in the elastomer domains of Figure 4a due to an inhomogeneous RuO_4 staining in the section. This may result from the underlying distribution of elastomer and iPcE in the dispersed domains. The presence of the iPcE lamellae within the elastomer domains and the apparent immiscibility of the component polymers in the solid state, ascertained from the temperatures of the relaxation events through DMA, suggest partial mixing in the melt state followed by phase separation upon cooling. The mottled texture, indicating an inhomogeneous distribution of materials, may be the signature of liquid–liquid phase separation arrested, and frozen-in, by the crystallization of the iPcE. The spherical inclusion seen in the bottom left of Figure 4a, of mean diameter 126 nm, is lightly stained material within the EcO domains. This feature is thought to be due to the presence of iPcE that was mechanically occluded during mixing, due to its regular shape and similar staining characteristics to the matrix phase, and hence the inclusions were probably not formed through phase separation.

Linear Polyethylene Samples

When the matrix was linear polyethylene, the morphology exemplified by the micrograph in Figure 5 taken from a sample injection molded at 230°C containing 27.9 wt% of EcO2 (= 30 vol% at 25°C) was obtained. It comprises an interpenetrating morphology of elastomer domains and lamellar crystals of PE. The lamellae were measured from the TEM micrographs to be around 17 nm

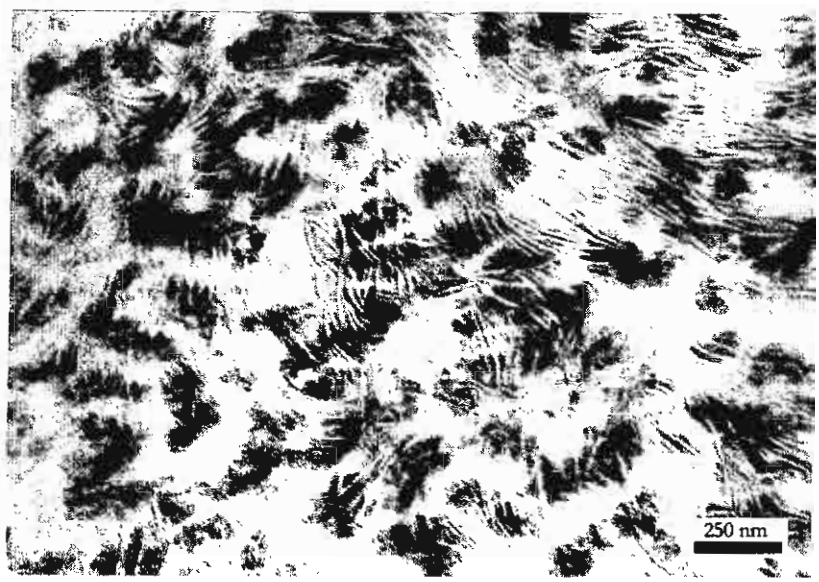

Figure 5. TEM micrograph showing the interpenetrating morphology found in the PE1 specimens, molded at 230°C and 0 Pa back pressure, containing 27.9 wt% of EcO2.

thick. A typical peak melting temperature, by DSC, of the blended PE, that was largely independent of elastomer contents lower than 30 wt%, was 129°C giving a predicted crystal thickness, according to the Gibbs-Thompson equation, of 19.6 nm; the data used in this calculation were the same as that used in the crystal thickness calculation of EcO. These results suggest that all lamellae situated in the EcO domains comprise linear PE, with no incorporation of the elastomer into the crystals. The Jordhamo equation (15) for co-continuity of phases in immiscible systems is

$$\frac{\eta_1}{\eta_2} \cdot \frac{\phi_2}{\phi_1} \cong 1,$$

where ϕ_1 and η_1 are the volume fraction and viscosity, respectively, of component 1. The viscosity ratio, η_{EcO}/η_{PE}, of these polymers is of the order of four at most processing conditions used, and hence the co-continuity point of the phases would not be anticipated until the elastomer content approaches a maximum random packing fraction of the order of 0.72. Evidently, howeverb, much lower elastomer contents result in interconnected morphologies. From the extensive penetration of PE lamellar crystals into the EcO domains, it may be concluded that a considerable quantity of the PE and EcO were mixed at the molecular level at the onset of crystallization. The predicted critical composition, ϕ_2^c, from the Flory-Huggins

lattice model (16),

$$\phi_2^c = \left(1 + (v_2 N_{w2}/v_1 N_{w1})^{1/2}\right)^{-1},$$

is at 35.2 vol% of EcO2 at 25°C, in the case of PE2; where $N_{w1} = M_{w1}/M_{01}$, M_{w1} is the weight average molecular weight, M_{01} is the molecular weight of the polymer repeat unit, v_1 is the molar volume of component 1 at temperature, T, and subscript 1 and 2 refer to PE and EcO, respectively. Under the melt flow, conjugate PE-rich and elastomer-rich phases may be formed that are sheared to a very fine length of mixing that reaches the molecular level. The interpenetrating morphology must be a consequence of the phase separation after the flow of a partially miscible melt. DMA data showed that the major relaxation event of the EcO in the toughened PE moldings was only 5°C higher than the same process in the pure resins, implying that the component polymers were largely de-mixed at the molecular level in the solid state. Under all molding conditions used, the melt must have been homogenized to a length-scale less than 170 nm. The coarsening processes during cooling generated the solid state morphology. Under quiescent conditions, the blend was found to be two-phase at the critical composition up to the limit of stability of the PE, that is around 375°C under a nitrogen atmosphere, and hence the critical temperature could not be determined. The injection molding

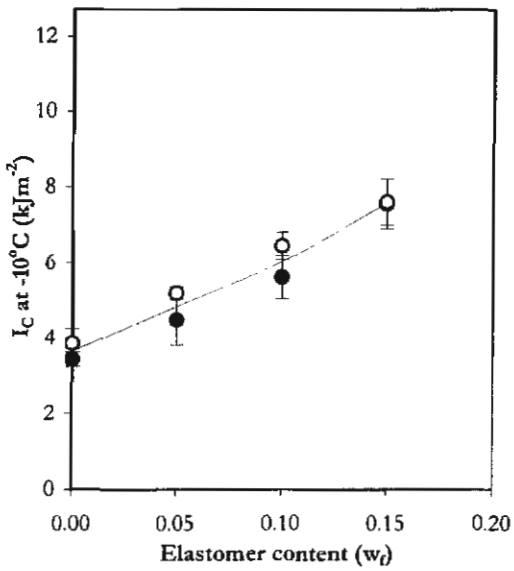

Figure 6. Charpy impact energies, I_C, at −10°C versus weight fraction of elastomer, wf, for the EcO2 toughened PE2 samples injection molded at (•) 170 and (○) 230°C. Error bars are ± the sample standard deviation.

conditions had a statistically significant, but technologically small, effect on the impact properties of the PE samples, as shown in Figure 6. In each condition, a very fine solid-state morphology of length-scale around 170 nm was obtained.

CONCLUSIONS

A range of solid-state morphologies were produced in the injection molded polyolefins toughened with poly(ethylene-co-1-octene) elastomer. The effect was thought to be related to the influence of melt-flow on the partially miscible melt particularly when the ethylene content of the matrix was increased. Immiscibility in the solid state was found in each case, and hence it was inferred that the solid state morphologies were in part determined by the progress of phase separation and the concurrent crystallization of the matrix phase on cooling after processing. For the iPP and iPcE systems, the impact properties were critically dependent on the injection molding conditions, with decreases in toughness associated with increased elastomer domain sizes at higher molding temperatures. For the PE that exhibited pronounced miscibility in the melt-state, differences in the processing conditions had a relatively minor influence on impact toughness.

ACKNOWLEDGMENTS

The authors would like to thank the Thailand Research Fund (TRF) for support.

REFERENCES

1. Walker, I.; Collyer, A.A. Rubber Toughening Mechanisms in Polymeric Materials. In *Rubber Toughened Engineering Plastics,* 1st Ed.; Collyer, A.A., Ed.; Chapman and Hall: London, 1994; 29–53.
2. Madbouly, S.; Ohmomo, M.; Ouzigawa, T.; Inoue, T. Polymer **1999**, *40*, 1465.
3. Kammer, H.W; Kummerlowe, C.; Kressler, J.; Melior, J.P. Polymer **1991**, *32* (8), 1488.
4. Inoue, T. Shear Induced Mixing in Polymer Blends, A Special Seminar Presented at the Faculty of Science, Mahidol University, Thailand, Dec 14, 1998.
5. Olley, R.H.; Basset, D.C. Polym. Commun. **1982**, *23*, 1707.
6. Morton-Jones, D.H. Mixing. In *Polymer Processing*, 1st Ed.; Chapman and Hall: London, 1989; 71.

7. Rauwendaal C. Important Polymer Properties. In *Polymer Extrusion*, 2nd Ed.; Hanser Publishers: Munich, 1990; 181.
8. Wu, S.J. Appl. Polym. Sci. **1988**, *35*, 549.
9. Varga, J. Crystallization, Melting, and Supermolecular Structure of Isotactic Polypropylene. In *Polypropylene Structure, Blends, and Composites: Structure and Morphology*, 1st Ed.; Karger-Kocsis, J., Ed.; Chapman and Hall: London, 1995; Vol. 1, 64.
10. Cheng, S.Z.D.; Janimak, J.J.; Rodriguez, J. Crystalline Structures of Polypropylene Homo- and Copolymers. In *Polypropylene Structure, Blends, and Composites: Structure and Morphology*, 1st Ed.; Karger-Kocsis, J., Ed.; Chapman and Hall: London, 1995; Vol. 1, 38.
11. Snyder, R.L. X-Ray Diffraction. In *Materials Science and Technology: A Comprehensive Treatment: Characterisation of Materials Part 1*, 1st Ed.; Lifshin, E., Ed.; VCH Verlagsgesellschaft: Weinheim, 1992; Vol. 2A, 290.
12. Gedde, U.W. *Polymer Physics;* Chapman and Hall: London, 1995.
13. Wunderlich, B. The Growth of Crystals. In *Macromolecular Physics: Crystal Nucleation, Growth, Annealing*, 1st Ed.; Academic Press: New York, 1976; Vol. 2, 154.
14. Varga, J. Crystallization, Melting, and Supermolecular Structure of Isotactic Polypropylene. In *Polypropylene Structure, Blends, and Composites: Structure and Morphology*, 1st Ed.; Karger-Kocsis, J., Ed.; Chapman and Hall: London, 1995; Vol. 1, 59.
15. Jordhamo, G.M.; Manson, J.A.; Sperling, L.H. Polym. Eng. Sci., **1986**, *26*, 517.
16. Crist, B.; Hill, M.J. Polymer, **1997**, *35*, 2329.

Melt-Flow-Induced Phase Morphologies of a High-Density Polyethylene/Poly(ethylene-*co*-1-octene) Blend

ARUNEE TABTIANG,[1] BOOTSARA PARCHANA,[1] RICHARD A. VENABLES,[1] TAKASHI INOUE[2]

[1] Department of Chemistry, Faculty of Science, Mahidol University, Rama VI Road, Bangkok 10400, Thailand

[2] Department of Organic and Polymeric Materials, Tokyo Institute of Technology, Ookayama, Megoru-ku, Tokyo 152, Japan

Received 23 July 1999; revised 15 October 2000; accepted 29 November 2000
Published online 2 January 2001

ABSTRACT: A blend of high-density polyethylene and an elastomeric poly(ethylene-*co*-1-octene) resin, containing 25 mol % octene and long-chain branching, was phase-separated in the melt under quiescent conditions. After melt flow, the blend had fine globular or interconnected phase morphologies that were interpreted as originating from the various stages of coarsening after liquid–liquid phase separation through spinodal decomposition. It was inferred that the miscibility of the blend was enhanced under melt flow. After cessation of flow, concurrent liquid–liquid and solid–liquid phase separation took place, resulting in the formation of an interpenetrating morphology comprising amorphous polyethylene, copolymer, and crystalline polyethylene. © 2001 John Wiley & Sons, Inc. J Polym Sci B: Polym Phys 39: 380–389, 2001
Keywords: polyolefin blend; miscibility; phase separation

INTRODUCTION

The miscibilities of polyolefin blends are strongly affected by the extent of short-chain and long-chain branching in each polymer. Short-chain branching is principally controlled by the types and quantities of the comonomers present; for example, propylene confers methyl branches, butene provides ethyl branches, and octene gives hexyl branches. A number of studies have described the partial miscibility of polyolefin blends containing polymers with different branch levels after annealing under quiescent conditions.[1,2] In some instances, olefinic copolymers have been shown to exhibit partial miscibility with polypropylene because of the entropic repulsion created in the copolymer caused by the dissimilarity of the comonomers.[3–5] Melt processing profoundly affects the morphology of polymer blends, particularly when the polymers approach the limits of miscibility.[6] At higher shear rates, flow-enhanced miscibility has been observed, whereas demixing has also been observed at lower shear rates. These phenomena have been reported for the polystyrene/poly(vinyl methyl ether)[7] and polycarbonate/poly(styrene-*co*-acrylonitrile) systems.[8] More recently, flow-enhanced miscibility has been observed in polyolefin blends under injection-molding conditions.[9] Theories explaining these experimental data include the additive effect of melt elasticity to the free energy of mixing,[10] changes in the specific interaction contacts where relevant, and the alteration of the entropy of mixing.[7] In most of the previous studies, light scattering was used to follow changes in the cloud points of blends under quiescent and shear flow conditions.[6,8] Several studies have reported the morphologies resulting from the melt processing of partially miscible blends. Okamoto et al.[8]

Correspondence to: R. A. Venables (E-mail: frrav@mahidol.ac.th)

Journal of Polymer Science: Part B: Polymer Physics, Vol. 39, 380–389 (2001)

showed highly interconnected morphologies involving both phases in injection-molded blends of polycarbonate with poly(styrene-*co*-acrylonitrile) that possessed regular domain spacing. It was inferred that this was the hallmark of spinodal decomposition; dissolution of the blend components was reported at a barrel temperature of 260 °C, 37 °C above the lower critical solution temperature, 223 °C. After cessation of flow, phase separation took place. Sano et al.[9] reported the morphologies in the skin region of injection-molded polypropylene/high-density polyethylene (HDPE; 60/40 w/w) blends prepared at 240 °C. In these samples, a regularly phase-separated structure comprising stripes with a periodic distance of around 0.15 μm was observed through transmission electron microscopy (TEM) of RuO_4-stained sections. In the micrographs, the bright areas consisted of crosshatched polypropylene lamellae, whereas the darker areas comprised polyethylene (PE) lamellae 10 nm thick. It was inferred that this morphology was the result of the depression of the upper critical solution temperature and/or the elevation of the lower critical solution temperature of the immiscible blend under the extreme flow conditions of up to 20,000 s^{-1} found in the injection molder. Although increases in the lower critical solution temperatures of around 50 °C have been measured through light scattering studies,[8] the results of Sano et al.[9] suggest that greater changes may be obtained for polyolefin blends. The direct study of polyolefin blends through light scattering is limited, however, because of the similarity of the refractive indices of the constituent polymers. Indirect studies through microscopy of quenched samples may offer an alternative route for investigating polyolefin systems.

In terms of volume of production, blends containing PEs may be viewed as the most important commercial group. Commercial linear low-density polyethylenes (LDPEs) are heterogeneous mixtures of lightly branched and highly branched copolymers of ethylene with α-olefins, most often 1-butene and 1-octene. Phase separation in these materials under quiescent conditions in the melt state has been reported.[11] The morphologies in the solid state and, hence, the properties (especially toughness) may be affected by the mixing and phase separation during processing. To investigate these phenomena under processing conditions, we performed the study presented here. In this report, the solid-state morphology of an HDPE/poly(ethylene-*co*-1-octene) copolymer (EOC) blend is presented, and some inferences concerning the scenario of phase behavior in the melt state under flow are drawn.

EXPERIMENTAL

The HDPE (Thai Polyethylene Co., Ltd., Thailand) had a melt-flow index of 18 g/10 min. The EOC, manufactured by Dow–DuPont elastomers with a single-site catalyst, had a melt-flow index of 0.5 g/10 min (melting point ≈ 50 °C); it contained 25 mol % octene and long-chain branching.[12] Further details of these resins are documented in Table I. HDPE/EOC blends (72/28 wt %) were prepared either through melt blending with a Prism 16-mm twin-screw extruder at a barrel temperature of 180 °C and a screw speed of 175 rpm or through solvent blending. In the latter case, the resins were dissolved in boiling toluene under nitrogen and then precipitated by being poured into excess methanol. The tensile specimens (BS 2782: Part 3, method 320A) were prepared from the melt blends with a Dr Boy 22S injection molder, with barrel temperatures of 170 or 230 °C; the screw speed was 100 min^{-1}, the back pressure was zero, and the cycle time was approximately 30 s. Selected moldings and the solution blends were annealed in an oil bath, after being wrapped in aluminum foil, for 15 min and 6 h, respectively; the temperatures were 170 and 230 °C. Specimens about 15 μm thick for the dynamic mechanical analysis (DMA) were sectioned from the skins of the injection moldings with a microtome. Analyses were carried out in tensile mode with a frequency of 10 Hz and a heating rate of 5 °C/min with a DMTA mkII thermal analyzer from Polymer Laboratories. Differential scanning calorimetry (DSC) data were obtained with a PerkinElmer DSC7 instrument; specimens (10 ± 0.1 mg) were cut from the central core of the moldings and dipped in silicone oil to ensure rapid heat transfer to the specimens. Fusion endotherms were obtained at a heating rate of 30 °C/min, to limit annealing during heating, under a nitrogen atmosphere. TEM micrographs were obtained from material at the skins and cores of the moldings. The samples were flattened with an RMC ultramicrotome at −100 °C and then stained in sealed tubes above a RuO_4 solution at 60 °C for 1 h. The staining procedure was repeated three times with fresh reagent. Finally, sections around 70 nm thick were obtained from the stained samples through ultramicrotomy at

Table I. Polymer Characteristics

Parameter	Polymer			Blend
	PE	P1O	EOC	(70/30 v_{PE}/v_{EOC})
C_∞	7.00[a]	9.10[a]	7.53[b]	—
b (nm)	0.815	0.929	0.845	—
M_w (g mol^{-1})	45,000	—	162,700	—
M_0 (g mol^{-1})	28.054	112.216	49.095	—
n	3,207	—	6,627	—
n_s	802	—	1,657	—
R_g (nm)	9.4	—	14.0	12.1
r (nm)	23.1	—	34.4	29.6
L (nm)	—	—	—	17.1
$V_{25\,°C}$ (cm^3 mol^{-1})	33.1[c]	130.8[c]	57.5	—
$\rho_{25\,°C}$ (g cm^{-3})	0.962[d]	—	0.868[d]	—
α (m^2 s^{-1}) $\times 10^7$	1.57[e]	—	1.17[e]	1.46[f]
$D_{170\,°C}$ (cm^2 s^{-1}) $\times 10^{10}$	1.28	—	0.22	0.36
$D_{230\,°C}$ (cm^2 s^{-1}) $\times 10^{10}$	2.82	—	0.71	1.10

[a] Reference 13.
[b] Data for EOC calculated from the copolymer composition weighted average of the values for PE and P1O.
[c] Reference 14.
[d] Typical density at 25 °C.
[e] Reference 15, assuming that α for EOC is equal to that of LDPE.
[f] Calculated from the mass fraction weighted average of the values for PE and EOC.

room temperature. Sections were floated onto copper grids and were observed with a Hitachi H-300 microscope. Light micrographs were obtained of microtomed sections taken from the annealed solution blends with a Nikon E400 transmitted light microscope. Surfaces that were flattened with the ultramicrotome at −100 °C were etched through immersion in permanganic acid for 24 h at 30 °C, coated with a platinum–palladium alloy, and viewed with a Hitachi S-2360N scanning electron microscope to obtain the number of spherulites per unit area in the cross section. Rheological data were collected with a Rosand capillary rheometer and a Haake RT20 parallel plate rheometer. Bagley and Rabinowitsch corrections were applied to the capillary rheometer data.

RESULTS AND DISCUSSION

Solution Blends

Figure 1 shows light micrographs of the solution blends after annealing at 170 and 230 °C for 6 h under quiescent conditions. At both temperatures, distinct, large phase domains are visible. Banded spherulites are seen in one phase, iden-

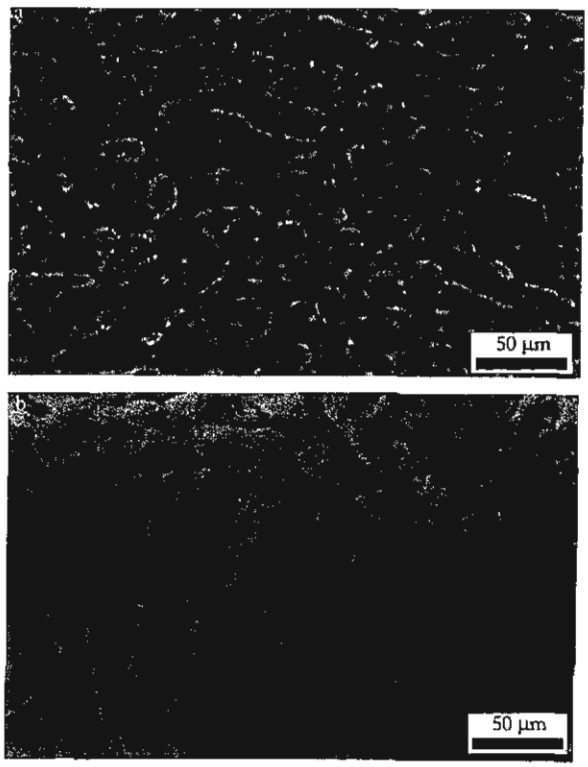

Figure 1. Light micrographs of the solution blends after annealing at (a) 170 °C and (b) 230 °C for 6 h.

tifying it as HDPE-rich. Einstein's diffusion equation relates the diffusion distance x to the diffusion rate D_{app} and the time for diffusion t: $\overline{x^2} = 2D_{app}t$. If D_{app} is 1.1×10^{-10} cm^2s^{-1}, x is 0.3 μm for a 5-s diffusion time. On the basis of the rapid quenching, within 5 s after annealing, the morphology is too coarse for it to result from phase separation during cooling, and so it is inferred that the melt was biphasic. Direct observation of phase separation in the melt was not achieved, however, because of the closeness of the refractive indices of the EOC and HDPE melts. In the solid state, the difference in density between the crystalline HDPE and the amorphous EOC provides contrast between the two phases. The area fraction of the EOC-rich phase is greater than that expected from the 28 wt % or 30 vol % at 25 °C EOC composition of the blend. Moreover, there is connectivity between the phase domains, rather than discretely dispersed droplets. A probable explanation is that a fraction of the HDPE dissolves into the EOC phase, thereby increasing its effective volume fraction and resulting in droplet coalescence and, hence, domain connectivity. These observations suggest some limited miscibility in the melt at both 170 and 230 °C. The extensive branching in the EOC precludes its cocrystallization with the HDPE, and so solid–liquid phase separation will occur as the HDPE crystallizes, leading to heterogeneity within the phase domains observed in Figure 1.

Melt Flow

An estimate of the flow history in the injection molder was obtained through the following analysis. The power dissipated per unit volume during plasticization, P, was taken as[16]

$$P = \eta^*(\dot{\gamma}_c)^2$$

where η^* is the complex viscosity at angular frequency ω. It was assumed that $\omega = \dot{\gamma}_c$, that is, the steady shear rate in the channel of the screw in the metering zone:[17]

$$\dot{\gamma}_c = \pi(D - 2h)N/h$$

where D is the internal barrel diameter (24 mm), N is the screw speed (100 min^{-1}), and h is the screw channel depth (2 mm); therefore, $\dot{\gamma}_c = 52$ s^{-1}. For the blend, η^* is 1296 and 585 Pa · s at 170 and 230 °C, respectively. The specific mechanical energy input during plasticization, S_e, was calculated as $S_e = Pt_p$, where t_p is the plasticization time (5 s): S_e is 17.5 MJ m^{-3} at 170 °C and 7.9 MJ m^{-3} at 230 °C. The shear rate at the wall of the nozzle, $\dot{\gamma}_N$, was estimated from[18]

$$\dot{\gamma}_N = (4Q/\pi r^3)(3n + 1)/4n$$

where $n = d \lg \tau / d \lg \dot{\gamma}$, $Q = v_{T,P}m/t_I$, Q is the melt injection rate, m is the shot weight (15 g), $v_{T,P}$ is the specific volume of the melt at temperature T and injection pressure P (3.4 MPa), t_I is the injection time (2 s), r is the radius of the nozzle orifice (1.25 mm), τ is the shear stress at the wall, and n is the non-Newtonian exponent. Both at 230 and 170 °C, $\dot{\gamma}_N \approx 6500$ s^{-1}, if specific melt volumes of 1.27 and 1.33 cm^3g^{-1} are assumed for melts at 170 and 230 °C, respectively, under 3.4 MPa of pressure.[19] A description of the cooling process in the injection moldings may be obtained with the Fourier equation for nonsteady heat flow in one dimension:[20]

$$\partial T/\partial t = \alpha(\partial^2 T/\partial x^2)$$

where T is the temperature, t is time, α is the thermal diffusivity, and x is the distance between the part of the molding in question and the mold surface. The thermal diffusivity is related to k, the thermal conductivity, ρ, the density, and C_P, the specific heat capacity: α is equal to $k/\rho C_P$; data are given in Table I. If the cooling of the melt at the mold surface may be described by one-sided heat conduction into a semi-infinite body and α is constant over the temperature change, an estimate of the cooling rate may be made. Two-sided heat transfer was used to describe the cooling of the core. The dimensionless Fourier parameter, F_0, is calculated as $F_0 = \alpha t/x^2$. In the core, x is half the molding thickness (x = 3.2 mm/2); in the skin region, x is the distance from the mold surface to where the TEM sections were obtained (0.1 mm). A plot of the temperature gradient, ΔT, where

$$\Delta T = (T_{x,t} - T_{ms})/(T_0 - T_{ms})$$

against F_0 for a flat sheet was used to find F_0 at ΔT, and so the time to reach $T_{x,t}$ may be found;[21] T_{ms} is the mold surface temperature (30 °C), T_0 is the initial melt temperature (230 or 170 °C), and $T_{x,t}$ is the temperature at x after time t. $T_{x,t}$ was taken as the estimated temperature where the crystal growth rate of PE is a maximum. This is[22]

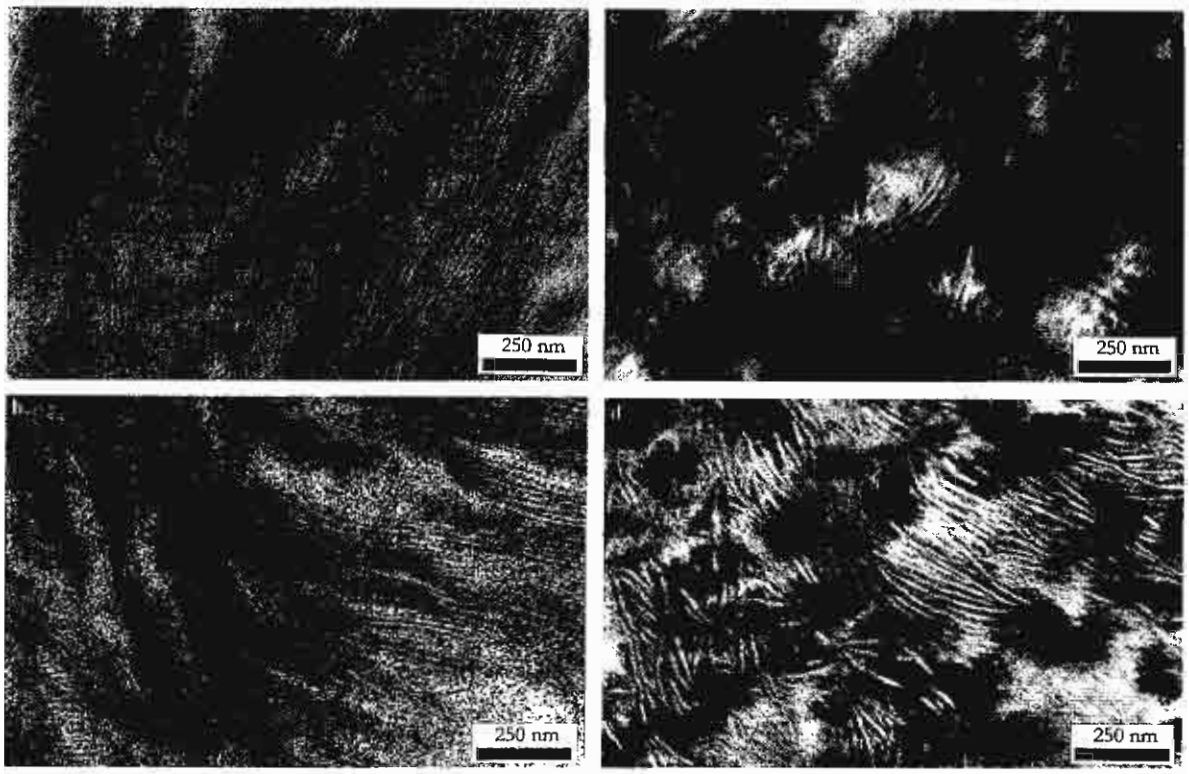

Figure 2. TEM micrographs of the as-molded specimens in the core region prepared at two temperatures: HDPE at (a) 170 °C and (b) 230 °C and the HDPE/EOC blend at (c) 170 °C and (d) 230 °C.

5,000 μm min^{-1} at 112 °C, that is, 30 °C below the equilibrium melting point of 142 °C. Thus, $T_{x,t}$ is 112 °C, and so for a melt temperature of 230 °C, ΔT is 0.41, F_0 is 0.46, and the time taken to reach 112 °C is 8.1 s in the core and 0.03 s at the skin. For the 170 °C melt temperature, the corresponding values are ΔT = 0.59 and F_0 = 0.31 and cooling times in the core and skin of 5.4 and 0.02 s, respectively. The crystallization process in the core was assumed to be zero-order, three-dimensional spherulite growth. The number of spherulite nuclei in the cross section of the core, N_A, was 1.06×10^{-2} μm^{-2}. This value was determined by point counting of the spherulite centers in the scanning electron micrographs of permanganic acid-etched surfaces. The number-average spherulite diameter in the cross section, D_{nA}, was 10.6 μm. The number-average diameter in volume, D_{nV}, was[23]

$$D_{nV} = (4/\pi)D_{nA}$$

The number of spherulite nuclei per unit volume, N_V, was

$$N_V = N_A/D_{nV}$$

N_v is 7.9×10^{-4} μm^{-3}. To reach a maximum random packing fraction at impingement of the spherulites, ϕ_{max} ($\approx$0.7), from[24]

$$\phi_{max} = N_V \pi D_{nV}^3/6$$

at a spherulite growth rate of 83 μm s^{-1}, the time taken was 0.07 s after 112 °C was reached. The time taken for the melt to solidify was the sum of the cooling time and crystallization time; at the end of this period, the morphology was effectively frozen. For the melt at 230 °C, the solidification time was 8.2 s in the core and 0.10 s at the skin. The corresponding values for the 170 °C melt were 5.5 and 0.09 s, respectively.

Flow-Induced Morphology

Figure 2 displays TEM micrographs of the core regions of the as-molded blends, prepared at 170 and 230 °C, together with images of the original

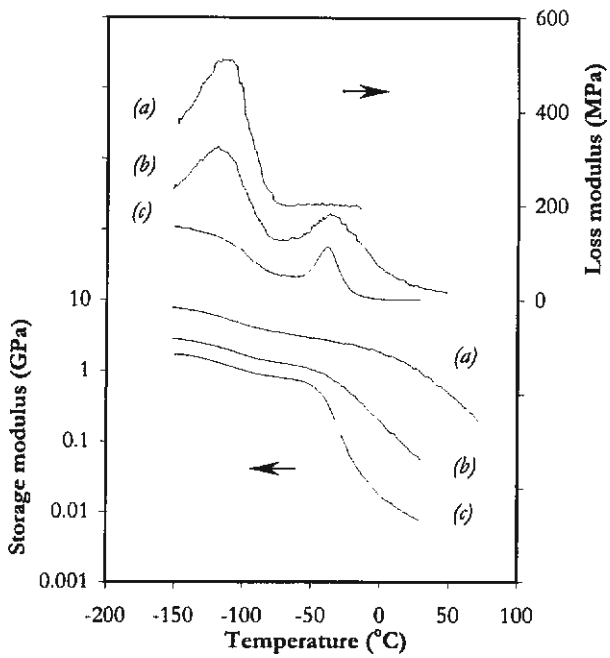

Figure 3. Typical DMA traces for (a) HDPE, (b) HDPE/EOC blend, and (c) EOC. The specimens were microtomed from the skins of the injection moldings; the loss modulus curves of the blend and PE are offset from the EOC curve by +50 MPa for clarity.

HDPE resin processed under comparable conditions. The near amorphous EOC constitutes the most heavily stained domains, whereas amorphous HDPE is more lightly stained; the HDPE lamellae are unstained. DMA traces of the HDPE resin, EOC, and the skin of a blend molding prepared at 230 °C are shown in Figure 3. The blend exhibits loss maxima at −115 and −32 °C that may be assigned to the glass transitions of HDPE and EOC, respectively. Although the glass-transition temperature of the original HDPE and the HDPE in the blends were essentially the same, for all injection-molded blends the glass-transition temperature of the EOC was 5–7 °C higher than that of the original EOC, that is, −37 °C; moreover, the relaxation peaks were slightly broader. In some locations in the blend, the EOC is pinned between neighboring HDPE lamellae; consequently, this may hinder its mobility, giving rise to the slight increase in the glass-transition temperature of the EOC. The peak broadening may result from the EOC being located both between the lamellae and in less confined domains that result in a distribution of local environments, each possessing different relaxation characteristics. The solid-state-phase domains largely comprise pure amorphous HDPE, pure EOC, and crystalline HDPE.

In the injection-molded blends, the EOC appears as an interconnected arrangement of globules that is intertwined with swathes of HDPE lamellae. The HDPE lamellae penetrate extensively into the EOC domains, indicating that crystals grew from or into a mixed phase containing both EOC and HDPE. The length scale of the EOC phase domains is very fine, with an average periodic distance in the EOC-rich areas of 154 nm. This morphology is unlikely to result simply from the mechanical work of dispersive mixing because the dynamic equilibrium of droplet breakup and coalescence confers a lower mean particle size limit for physical dispersive mixing in polymer blends of around 0.5 μm, although smaller domains are possible in reactive systems. Thus, it is inferred that the fine morphology is the product of concurrent liquid–liquid and solid–liquid phase separation from a mixed or partially mixed melt and, hence, that the flow during injection molding enhances the miscibility of the blend. Bicontinuous morphologies are evident in the image of the core of a molding prepared at 170 °C, displayed in Figure 4. The effects of the local cooling conditions in the mold are illustrated by the differences in the skin and core morphologies of the blend molded at 230 °C, shown in Figure 5. At the skin, the EOC is more evenly distributed, whereas in the core the EOC domains are larger and more distinct from the HDPE-rich areas. Moreover, the HDPE lamellae are thinner and less well defined in the skin.

A description of the morphology evolution may be obtained through the following discussion. The statistical segment length, b, is given by

$$b = (C_\infty n L^2/n_s)^{1/2}$$

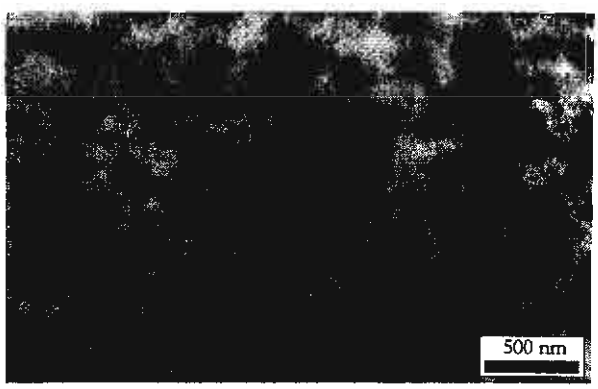

Figure 4. Overview of the EOC domain morphology in the core region of a blend molded at 170 °C.

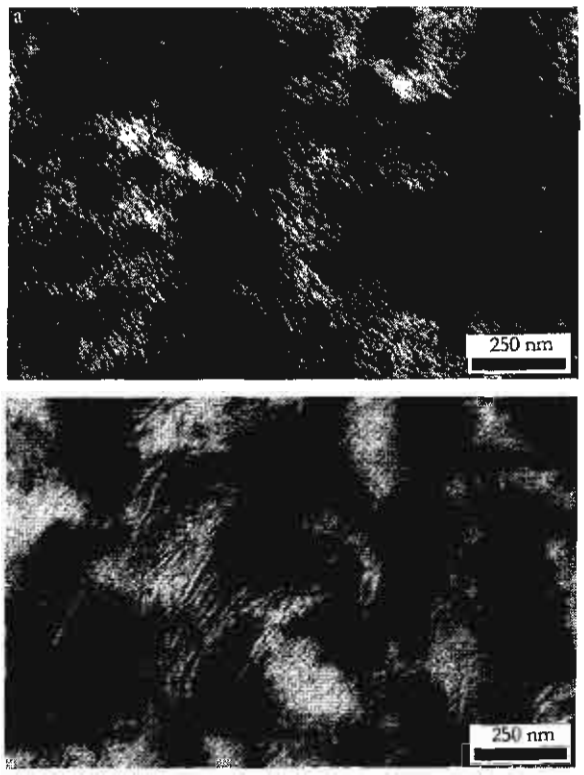

Figure 5. TEM micrographs of (a) skin and (b) core areas of a blend molded at 230 °C.

where n is the number of backbone carbons, $n = (2M_w/M_0) - 1$; n_s is the number of statistical segments based on a four-carbon unit, $n_s = (M_w/2M_0)$; M_w is the weight-average molecular weight; M_0 is the molecular weight of the polymer repeat unit; L is the C—C bond length (0.154 nm), and C_∞ is the characteristic ratio. R_g and r are the root mean square radius of gyration and root mean square end-to-end distance of the polymer chain, respectively:[25] $R_g = b(n_s/6)^{1/2}$ and $r = b(n_s)^{1/2}$ or $r = 6^{1/2}R_g$. These data are summarized in Table I; data for the ECO were calculated from the molar fraction weighted averages of the experimental data obtained for PE and poly(1-octene). The radius of gyration for a mixture of polymers 1 and 2, where polymer 1 is PE and polymer 2 is EOC, is given as follows:[26]

$$R_g = \left(\frac{n_{s(1)}n_{s(2)}(\phi_2 b_1^2 + \phi_1 b_2^2)}{6(\phi_1 n_{s(1)} + \phi_2 n_{s(2)})}\right)^{1/2}$$

where ϕ_j is the volume fraction of polymer j. The polymer–polymer interaction length, L, is determined as $L = r/3^{1/2}$; the kinetically favored length scale for demixing, λ_m, is related to the demixing temperature, T, and the temperature at the spinodal, T_s, from[27]

$$\lambda_m/L = 2\pi(3|T - T_s|/T_s)^{-1/2}$$

The 70/30 v_{PE}/v_{EOC} blend was found to be two-phase in the quiescent melt at all temperatures investigated, that is, from 150 to 350 °C. Limited miscibility for EOC contents of 10 vol % and lower was found at 350 °C. The critical point, ϕ_2^c is

$$\phi_2^c = (1 + (v_2 n_2/v_1 n_1)^{1/2})^{-1} = 0.35$$

where v_j is the monomer volume of component j. Extrapolation of the cloud-point curve to ϕ_2^c gave an approximate T_s of 400 °C; the corresponding λ_m values for demixing at 230 and 170 °C would be 95 and 82 nm, respectively. That is, λ_m decreases with increasing quench depth in a system with an upper critical solution temperature. The observed value of λ in the blend prepared at 230 °C was 154 nm. The growth rate of fluctuations, $R_{q(t)}$, at scattering vector q, is included in the following expression:

$$I_{q(t)} = I_{q(t=0)}\exp 2R_{q(t)}$$

where q_m is $2\pi/\lambda_m$ and $I_{q(t)}$ is the Fourier component, or scattering intensity, at q and time t. The maximum growth rate, R_m, is

$$R_m = q_m^2 D_{app}/2$$

The mutual diffusion coefficient, D_{app}, is

$$D_{app} = \frac{D_1 D_2(\phi_1 n_{s(1)} + \phi_2 n_{s(2)})}{\phi_1 n_{s(1)} D_1 + \phi_2 n_{s(2)} D_2} f$$

where D_j is the self-diffusion coefficient of polymer j, $D_j = k_j M_{(j)}^{-2}$; M is the molecular weight; and f is a factor that describes the slowing of diffusion as the spinodal temperature is approached. In the specimens described herein, the quench is relatively deep, that is, $|T_s - T| \geq 200$ °C, and so no slowing is considered. The temperature dependence of D_j is

$$D_j/T = Ae^{-E_{D/T}/RT}.$$

For linear PE,[28] $E_{D/T}$ is 24 kJ mol^{-1} and k 0.26 cm^{2}g^{2}mol^{-2}s^{-1}. These values are not known for EOC, so values were estimated from the data of

Bartels et al.[29] for poly(ethylene-*co*-1-butene). The calculated growth rates at 230 and 170 °C are 23.9 and 10.6 s^{-1}, respectively. The growth exponent is the product of R_m and the time allowed for growth, t; in this case, t was taken as the solidification time of the molding. $R_m t$ values at the skin and core for the melt at 230 °C are 2.4 and 196, respectively; at 170 °C, the corresponding values are 1.0 and 58. The early stages of coarsening may be considered as $R_m t \leq 1.1$. Thus, the morphology observed in the core region may have coarsened beyond the early stage, so q decreases below q_m and λ is greater than λ_m, whereas at the skin, the texture may be a result of the freezing of the early stage of phase separation.

Figure 6 shows the globular core morphology of the 230 °C as-molded melt blend, alongside the same molding after annealing at 230 °C for 15 min. In the melt under quiescent conditions, the EOC domains coalesce and occlude some of the HDPE-rich phase, suggesting that this fraction of the HDPE does not redissolve into the EOC under static conditions. Details of the domains in the blend molded at 170 °C and annealed at 170 °C for 15 min are displayed in Figure 7. HDPE lamellae can be seen penetrating into the EOC domain, from which it is inferred that some HDPE was mixed with the EOC under quiescent conditions in the melt. The extent of interpenetration is considerably less than that seen in the melt blend, however, and so it is concluded that the melt flow in the injection molder drives the blend toward miscibility. The spinodal boundary, which may be an upper and/or lower critical solution temperature type, may be shifted because of the melt flow. After cessation of flow and cooling, phase separation occurred rapidly and was complete within the cooling stage of the molding cycle. From the connectivity of the minor phase and the rapidity of the molding cycle, phase separation is likely to have occurred through spinodal decomposition. Moreover, the shape and arrangement of the EOC domains are consistent with this mechanism. The length scales of the observed morphologies are of the order of magnitude expected from phase separation on the basis of estimates of the molecular dimensions.

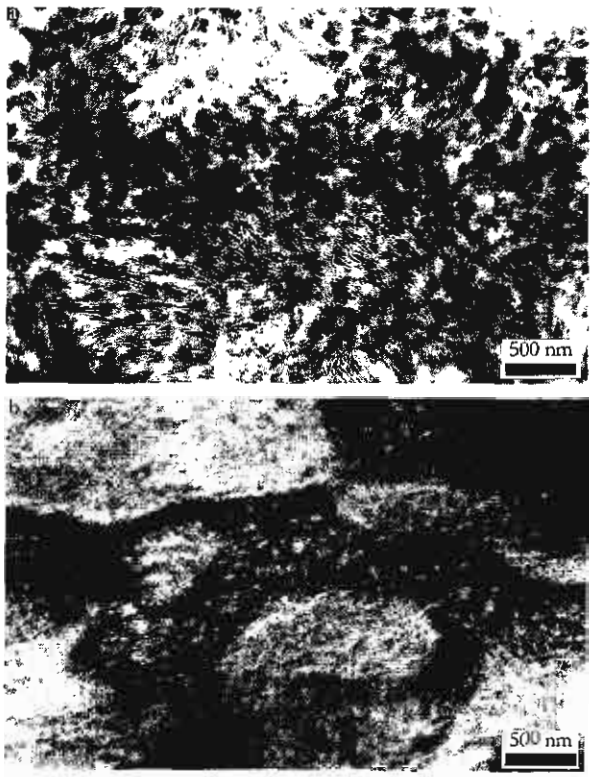

Figure 6. Core region of a blend molded at 230 °C: (a) as molded and (b) after annealing at 230 °C for 15 min.

Lamellar Morphology

In the molded blends, the HDPE lamellae penetrate the EOC-rich areas and extend into the HDPE-rich phase. Moreover, the highly stained regions at the edges of the lamellae show strong contrast with the unstained crystalline material because of the concentration of the EOC at these locations. The extensive chain branching in the EOC precludes its incorporation into the HDPE lamellae; consequently, as the HDPE crystallizes from the mixed phase, the EOC collects at the edges of the lamellae. This is further evidence that the polymers were mixed in the melt. The presence of EOC between the HDPE lamellae results in a distribution of the long-period values, ranging from around 18 nm in HDPE-rich areas to 27 nm in EOC-rich regions, although there is little change in the average lamellar thickness between the blend and the original HDPE prepared at the same molding temperature. This indicates that the melt was not homogeneous at the onset of crystallization, with the more closely packed lamellae forming from HDPE-rich regions and the thicker interlamellar regions the product of crystallization from areas with higher EOC concentrations. As the melt cools from above 200 °C through the spinodal boundary, liquid–liquid phase separation will begin and will continue unperturbed until HDPE crystallization begins at

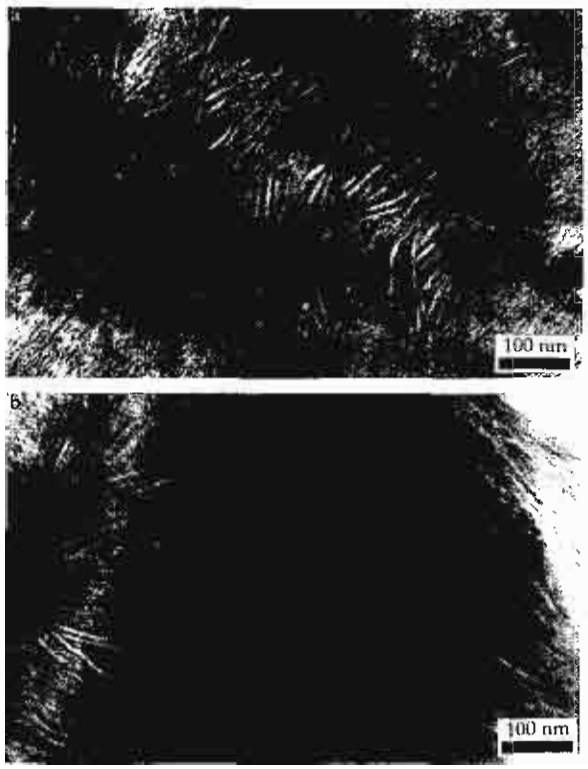

Figure 7. Detail of the phase domains of a blend molded at 170 °C: (a) as molded and (b) after annealing at 170 °C for 15 min.

temperatures below about 120 °C. At this point, HDPE lamellae grow rapidly from both EOC-rich and HDPE-rich areas. With close inspection of the PE lamellae in the melt blends in Figure 2, it is evident that the lamellae are not as straight as those seen in the original HDPE moldings, with some exhibiting an abrupt kink, whereas others have a more gentle wave conformation. This may be caused by the presence of EOC impurity in the HDPE melt during crystallization. The overall crystallinity of the HDPE, as determined through DSC, was significantly affected neither by molding temperature nor by liquid–liquid phase separation, because all determinations fell in the range 62.4–62.8%.

CONCLUSIONS

Melt flow during processing of the HDPE/EOC blend, which is partially miscible under quiescent conditions, resulted in the formation of a fine-length-scale morphology comprising intertwined HDPE lamellae and EOC domains. It may be inferred that the morphology resulted from the concurrent liquid–liquid and solid–liquid phase separation that occurred after cessation of flow and cooling.

R. A. Venables thanks the Thailand Research Fund, and A. Tabtiang thanks the Japan Society for the Promotion of Science program for its support of this work. R. A. Venables, A. Tabtiang, and B. Parchana express thanks to Professor Tadashi Komoto for help with the TEM reagent preparation and the donation of RuO_2, Koon Somrit Nilwanna (Hollywood Co., Ltd., Thailand) for the loan of the OM 35-mm camera, Tsuneo Chiba for advice in ultramicrotomy, Chemical Innovation Co., Ltd. (Thailand) for the donation of the elastomer, and Koon Wichai for help with the TEM work.

REFERENCES AND NOTES

1. Hill, M. J.; Barham, P. J. Polymer 1995, 36, 3369.
2. Hill, M. J.; Barham, P. J.; Keller, A. Polymer 1992, 33, 2530.
3. Otsuka, N.; Yang, Y.; Saito, H.; Inoue, T.; Takemura, Y. Polymer 1998, 39, 1533.
4. Lee, C. H.; Saito, H.; Inoue, T. Macromolecules 1995, 28, 8096.
5. Yamaguchi, M.; Nitta, K.; Miyata, H.; Masuda, T. J Appl Polym Sci 1997, 63, 467.
6. Hindawi, I. A.; Higgins, J. S.; Weiss, R. A. Polymer 1992, 33, 2522.
7. Katsaros, J. D.; Malone, M. F.; Winter, H. H. Polym Eng Sci 1989, 29, 1434.
8. Okamoto, M.; Shiomi, K.; Inoue, T. Polymer 1995, 36, 87.
9. Sano, H.; Yui, H.; Inoue, T. Polymer 1998, 39, 5265.
10. Kammer, H. W.; Kummerlowe, C.; Kressler, J.; Melior, J. P. Polymer 1991, 32, 1488.
11. van Ruiten, J.; Boode, J. W. Polymer 1992, 33, 2548.
12. DuPont–Dow Elastomers Product EG8150 Data Sheet; The Dow Chemical Company: Midland, USA. Aug 1996.
13. Bicerano, J. Prediction of Polymer Properties; Marcel Dekker: New York, 1993; Chapter 12, p 286.
14. Bicerano, J. Prediction of Polymer Properties; Marcel Dekker: New York, 1993; Chapter 3, p 66.
15. Crawford, R. J. Plastics Engineering, 2nd ed.; Pergamon: Oxford, 1987; Chapter 1, p 33.
16. Morton-Jones, D. H. Polymer Processing; Chapman & Hall: London, 1989; p 71.
17. Rauwendaal, C. Polymer Extrusion, 2nd ed.; Hanser: Munich, 1990; Chapter 6, p 181.
18. Nielson, L. E. Polymer Rheology; Marcel Dekker: New York, 1977; Chapter 1, p 16.

19. Grulke, E. A. Polymer Process Engineering; PTR Prentice Hall: Englewood Cliffs, New Jersey, 1994; Chapter 10, p 577.
20. Crawford, R. J. Plastics Engineering, 2nd ed.; Pergamon: Oxford, 1987; Chapter 5, p 279.
21. Crawford, R. J. Plastics Engineering, 2nd ed.; Pergamon: Oxford, 1987; Chapter 5, p 280.
22. Progelhof, R. C., Throne, J. L. Polymer Engineering Principles; Hanser: Munich, 1993; Chapter 2, p 129.
23. Dehoff, R. T. Quantitative Microscopy; McGraw-Hill: New York, 1968; Chapter 5, p 131.
24. Wypych, G. Fillers; ChemTec: Toronto-Scarborough Ontario, Canada, 1993; Chapter 4, p 143.
25. Gedde, U. W. Polymer Physics; Chapman & Hall: London, 1995; Chapter 2, p 21.
26. Rhee, J.; Crist, B. Macromolecules 1991, 24, 5663.
27. Olabisi, O.; Robeson, L. M.; Shaw, M. T. Polymer–Polymer Miscibility; Academic: New York, 1979; Chapter 2, p 46.
28. Klein, J.; Fletcher, D.; Fetters, L. J. Faraday Symp Chem Soc 1983, 18, 159.
29. Bartels, C. R.; Crist, B.; Graessley, M. W. Macromolecules 1984, 17, 2702.